

Chapter 2

Advanced Control of Photovoltaic and Wind Turbines Power Systems

Yongheng Yang, Wenjie Chen and Frede Blaabjerg

Abstract Much more efforts have been made on the integration of renewable energies into the grid in order to meet the imperative demand of a clean and reliable electricity generation. In this case, the grid stability and robustness may be violated due to the intermittency and interaction of the solar and wind renewables. Thus, in this chapter, advanced control strategies, which can enable the power conversion efficiently and reliably, for both photovoltaic (PV) and wind turbines power systems are addressed in order to enhance the integration of those technologies. Related grid demands have been presented firstly, where much more attention has been paid on specific requirements, like Low Voltage Ride-Through (LVRT) and reactive power injection capability. To perform the functions of those systems, advanced control strategies are presented with much more emphasis on the LVRT operation with reactive power injection for both single-phase and three-phase systems. Other control strategies like constant power generation control for PV systems to further increase the penetration level, and the improvements of LVRT performance for a doubly fed induction generator based wind turbine system by means of hardware protection solutions are also discussed in this chapter.

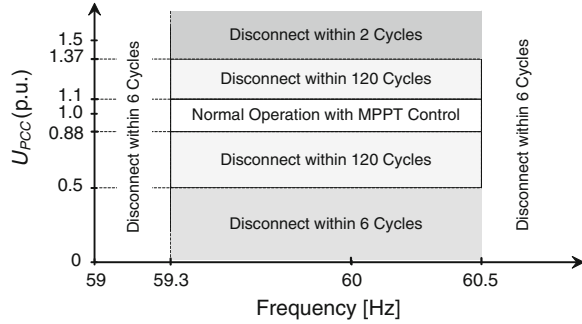
1 Introduction

Driven by a steady demand of clean and reliable electricity generation from renewable energy systems (e.g. photovoltaic and wind turbine systems), the grid requirements regarding the integration of renewable energy systems are going to

Y. Yang (✉) · F. Blaabjerg
Aalborg University, Aalborg, Denmark
e-mail: yoy@et.aau.dk

W. Chen
Zhejiang University, Hangzhou, China

Fig. 1 Example of the voltage and frequency window for PV systems in IEEE Std 929–2000 [1]



be more stringent, and thereby also the control systems. Thus, in this chapter, specific requirements for photovoltaic and wind turbine power systems are addressed firstly. Focuses are put on the advanced and intelligent control solutions for those systems to ensure an efficient and reliable electricity generation both from PV and wind turbine systems.

1.1 Grid Requirements for Photovoltaic Systems

Until currently, in most countries, the photovoltaic (PV) systems still account for a minor part of the overall electricity generation. Therefore, the Distribution/Transmission System Operators (DSOs/TSOs) impose basic grid requirements (i.e. grid codes) on those systems in order to guarantee the quality of the generated power. For example, in IEEE Std 929-2000, the Total Harmonic Distortion (THD) for the injected grid current should be lower than 5 % in normal operation to avoid adverse effects on other equipment connected to the grid [1–3]. Moreover, the boundaries of the grid voltage and frequency are also specified as shown in Fig. 1. In response to abnormal grid conditions, the PV systems are currently required to disconnect from the distributed grid for safety reasons, also known as the islanding protection. Whilst, in normal operation, the PV systems should maximize the output power, known as Maximum Power Point Tracking (MPPT).

With the rapid growth of low-voltage PV systems, the current active grid codes are expected to be modified in order to accept more PV energy in the grid [4, 5]. For the next generation PV systems, it is better to provide ancillary services, such as Low Voltage Ride-Through (LVRT), reactive power control and frequency control through active power control, in order to ensure reliable and efficient power conversion. Similar requirements are currently active for medium- and/or high-voltage applications (e.g. MW wind turbine systems and large PV power plant). For example, in Italy, it is required that the PV generation units serving low-voltage grid with the nominal power exceeding 6 kW have to ride through grid voltage faults [6]. In Germany, the medium- and/or high-voltage systems should have LVRT capability with reactive power injection [7]. Recently, a study

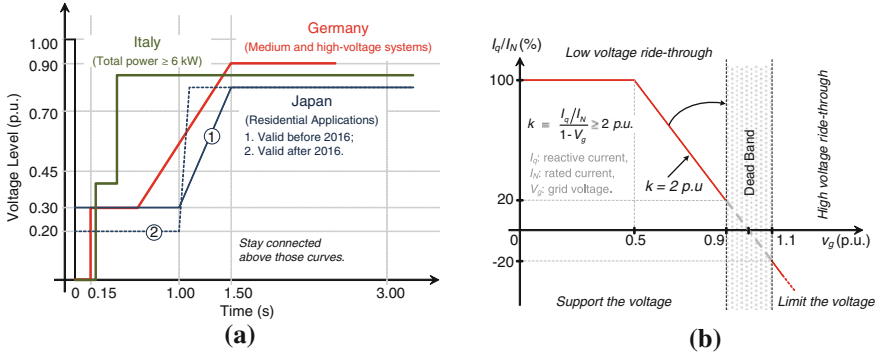


Fig. 2 **a** Low voltage ride-through requirements in different countries and **b** reactive current injection requirements during low voltage ride-through defined in E.ON grid code for medium and high voltage systems [7]

done in Japan presented the LVRT requirements on PV systems, which are connected to single-phase low-voltage grids [8]. Thus, the DSOs have given priority to find a solution in order to guarantee stable operation of distributed power systems and accept more PV energy. Examples of the requirements are shown in Fig. 2 [7]. Those requirements are imposed to ensure the safety of utility maintenance personnel, to protect the equipment, and also to guarantee utility stability.

Further increasing the PV penetration level can be achieved if the above ancillary services are adopted appropriately. Another solution to accept more PV energy is to reduce the maximum feed-in power from PV systems (e.g. 80 % of the nominal power) since the cut-off energy in a year is limited (e.g. 6.23 % reduction of total energy yield in Aalborg). By doing so, the distributed line capacity is also freed up. Recently, these issues have been discussed in some countries with a high penetration level of PV systems [9], e.g. Germany. In Sect. 2, control strategies are proposed and discussed in order to fulfil the above specific grid requirements.

1.2 Grid Requirements for Wind Turbine Systems

A general demand of the grid requirements for the wind power systems is that the Wind Turbine Systems (WTS) should behave as the synchronous generators based conventional power plants. During normal operation, the WTS is required to generate active and reactive power within a range around the rated voltage and frequency. The active power response speed and the reactive power capacity are restricted as well. Under grid faults, the WTS should remain connected to the grid and provide reactive power to support the grid, also referred as Fault Ride Through (FRT) requirements. The following provides a brief introduction of the grid requirements in a few countries.

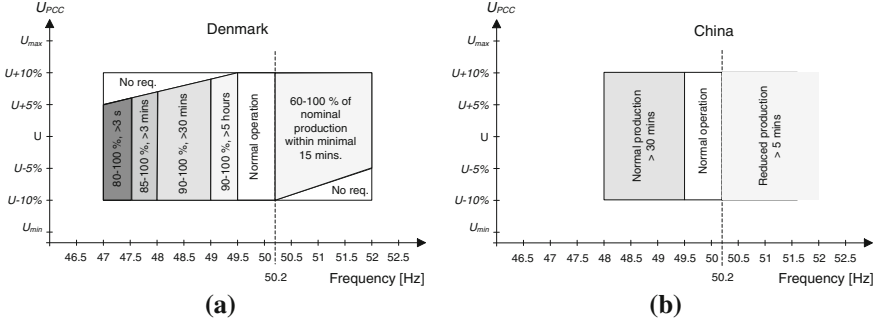


Fig. 3 Examples of voltage-frequency operation windows for WTS in **a** Denmark and **b** China

1.2.1 Grid Requirements for WTS Under Normal Operation

The grid requirements under normal operations include the frequency and voltage deviation, the active power control and the reactive power control. The requirements related to the frequency and voltage deviation demand that the WTS should operate within a range around rated voltage and frequency. Usually, this requirement can be described using three zones: (a) continuous operation zones, (b) time-limited operation zones, and (c) immediate disconnection zones, as it is shown in the example in Fig. 3 [10, 11].

The requirements on active power control demand the WTS must be equipped with active power constraint function, for example, keeping the active power constant during wind speed changes or limiting the ramp rate of the active power. In Denmark [10], three constraint functions are required for the WTS, including the absolute production constraint, the delta production constraint and the power gradient constraint.

The reactive power control requirement demand the wind power plants should regulate the output reactive power Q in response to the grid voltage variation, also known as Automatic Voltage Regulation (AVR). In general, the reactive power requirement is usually given in three different ways:

- Q control. The reactive power should be controlled independently of the active power at the point of connection.
- Power factor control. The reactive power is controlled proportionally to the active power at the point of connection.
- Voltage control. It is a function, which controls the voltage in the voltage reference point by changing the reactive power generation.

It should be noticed that the reactive power control and voltage control functions are mutually exclusive, which means that only one of the above three functions could be activated at a time.

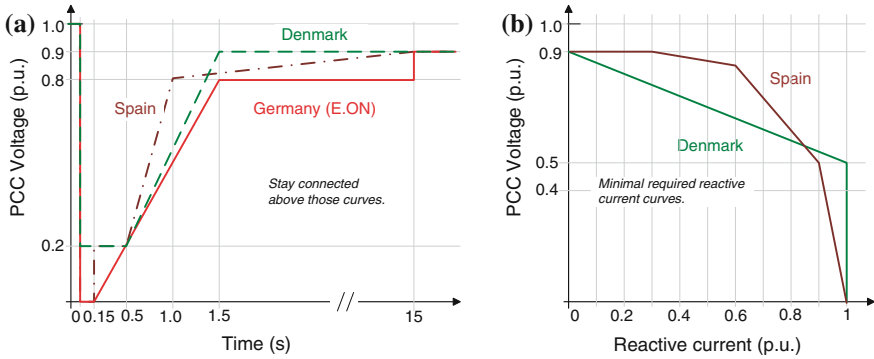


Fig. 4 **a** Low voltage ride-through requirements in different counties and **b** reactive current injection requirements during low voltage ride-through defined in Denmark and Spain

1.2.2 Grid Requirements for WTS Under Grid Faults

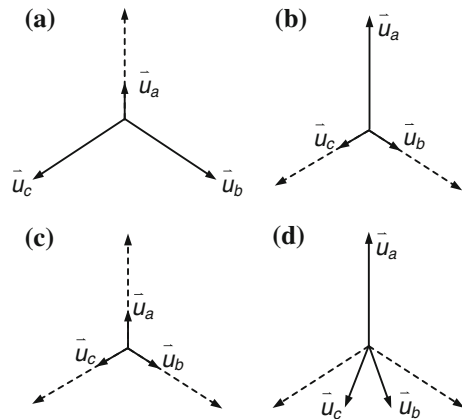
Grid faults will introduce grid voltage sags and/or swells. As more wind power plants have been connected to the grid, the grid code requires that the WTSs have to ride through grid faults for the stability concerns of the power system [5–7, 10–14]. The general requirements can be described as three aspects. (a) The WTS should remain connected during a short time of grid voltage sags and swells, known as LVRT and High Voltage Ride-Through (HVRT), respectively. (b) The WTS should provide an amount of reactive power to support the grid recovery. (c) After the fault clearance, the production of active power should be resumed at a limited rate.

LVRT Requirement

Voltage sags, due to short-circuited faults, are the most common grid faults in a power system. The voltage profiles in Germany, Denmark and Spain are shown in Fig. 4a under grid faults. The German and Spanish grid codes require that the WTSs should ride through zero voltage faults within 0.15 s, while the Danish grid code requires the WTS to ride through voltage sags with 20 % remaining voltage. The WTSs should stay connected to the grid when the voltage levels are above the curves.

Associated with the LVRT requirement, it is also stated in those grid codes (e.g. E.ON., Danish and Spanish grid codes in Figs. 2b and 4b) that the WTS should provide active and/or reactive power during the voltage dips. Normally, the reactive power support must be satisfied with the highest priority during a fault operation. The active power generation can be reduced in order to fulfill this requirement. The reactive power support requirements may differ with grid fault types in three-phase systems (e.g., three-phase fault, two-phase fault, etc.). For example, in Germany, the minimum reactive current under three-phase fault is 1.0 p.u.; while under single- and two-phase fault, the minimum reactive current is only 0.4 p.u.. Typically, the grid sags can be categorized into four fault types as they are shown in Fig. 5.

Fig. 5 Typical voltage sag types in three-phase systems
a single-phase-to-ground fault, **b** two-phase-to-ground fault, **c** three-phase-to-ground fault, **d** phase-to-phase fault



HVRT Requirement

Besides voltage dips, voltage swells are also observed in three-phase systems due to grid faults. Thus, the grid codes specify that the WTS should ride through a short time of high voltage, and at the same time absorb a certain reactive power for the stability concern, referred as HVRT. Figure 6a shows the HVRT requirements for WTSs in Germany and Spain [12, 13]. It is required for WTS to keep connected for at least 0.1 s, if the voltage at the Point of Common Coupling (PCC) reaches to 120 % of its normal value in Germany; while in Spain, the WTS should stay connected to the grid for 0.15 s under a 130 % voltage swell situation.

Similar to the LVRT operation, the WTS have to provide reactive power support to the grid during HVRT. However, instead of delivering reactive power to the grid, the WTS should absorb reactive power during HVRT operation in order to alleviate the voltage rise at PCC, as it is represented in Fig. 6b. The German grid code demands the WTS to absorb at least 1.0 p.u. reactive current during under a 120 % voltage swell situation; while in Spain, the requirement is to absorb about 0.73 p.u. reactive current under a 130 % voltage swell condition.

Recurring Fault Ride-Through

Recurring fault is also a challenge for the WTSs. Thus, the Danish grid has defined that the WTSs should withstand the recurring faults as it is summarized in Table 1 [10], and also illustrated as Fig. 7. The WTS capacity has to be sufficient to comply with the requirements specified in Table 1 if at least two independent faults specified in Table 1 occur within 2 min. The energy provided by auxiliary equipment should be sufficient in order to operate under at least six independent faults specified in Table 1 with time intervals of 5 min [10].

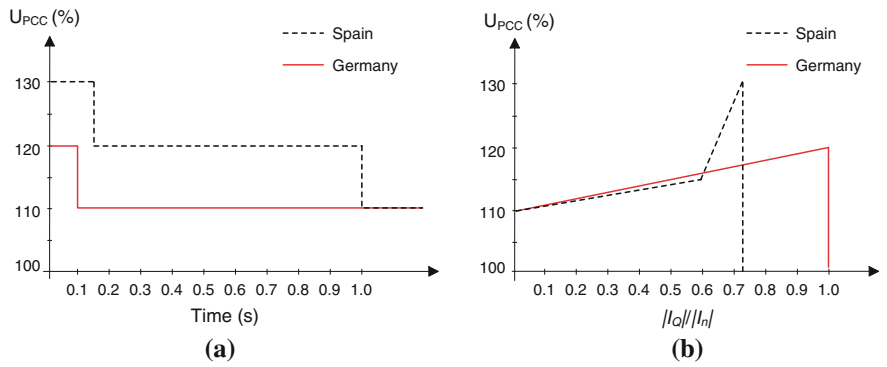
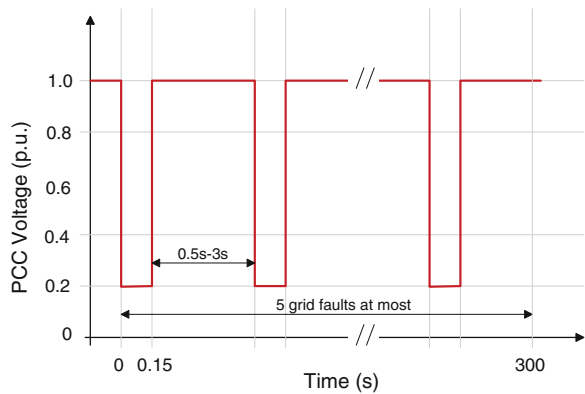


Fig. 6 **a** HVRT requirements for WTS and **b** reactive power requirements during HVRT in Germany (E.ON) and Spain

Table 1 Fault types and durations in the public electricity supply network in Denmark

Type	Fault duration
Three-phase short-circuit	Short-circuit for a period of 150 ms
Two-phase short-circuit with/without earth contact	Short-circuit for a period of 150 ms followed by a new short-circuit fault of 150 ms after 0.5–3 s
Single-phase short-circuit to earth	Single-phase-ground fault of 150 ms followed by a new single-phase-ground fault with the same duration after 0.5–3 s

Fig. 7 Voltage profile of recurring faults in the Danish grid code



2 Control of Photovoltaic Power Systems

Currently, the PV systems are dominantly for residential applications with low power ratings (single-phase, a few kW) and still account for a limited power generation in most countries. Underpinned by modern advanced power electronics

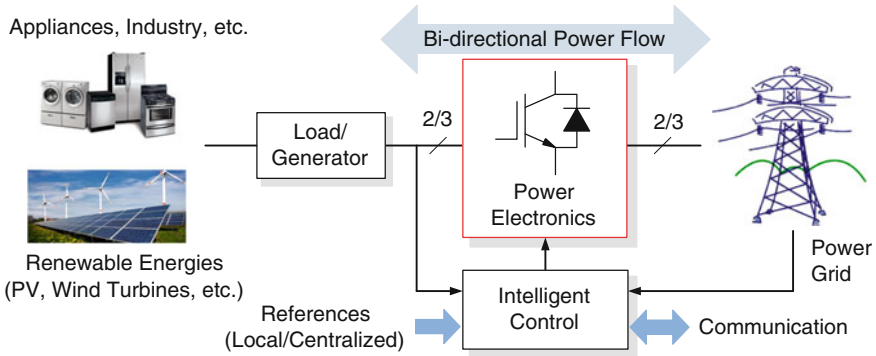


Fig. 8 Advanced modern power electronics technologies and intelligent control techniques to enable an efficient and reliable power generation from renewable energy sources

technologies, the penetration degree of those low-voltage PV systems is increasing in recent decades. Thus, ancillary services provided by PV systems are proposed in some countries [3–5]. As it is shown in Fig. 8, the power electronics converters together with intelligent control techniques in the renewable generation systems (PV systems and wind turbine systems) have this responsibility to enable the power conversion effectively and efficiently.

For a power-electronics based system as shown in Fig. 8, the power converters associated by intelligent control techniques are responsible for:

- Reliable/secure power supply,
- High efficiency, low cost, small volume, and effective protection,
- Control of active and reactive power injected into the grid, and
- Dynamic grid support (ride-through operation) and monitoring.

Therefore, in this section, advanced and intelligent control technologies of single-phase PV systems in the provision of ancillary services are discussed firstly. An overview of three-phase PV systems control technologies is presented as well. Since the injected current from a grid-connected converter is normally required to be synchronized with the grid voltage, the synchronization techniques are also discussed, together with the grid monitoring, which can improve the performance of grid-connected power converters.

2.1 Control of Single-Phase Photovoltaic Systems

Figure 9 presents the overall control diagram and functions that a PV system should provide. As for residential applications, typically, the power ratings range from 3 to 10 kW, and thus a DC/DC converter is necessary to boost the DC voltage level within an allowable range for the PV inverter (e.g. DC voltage range:

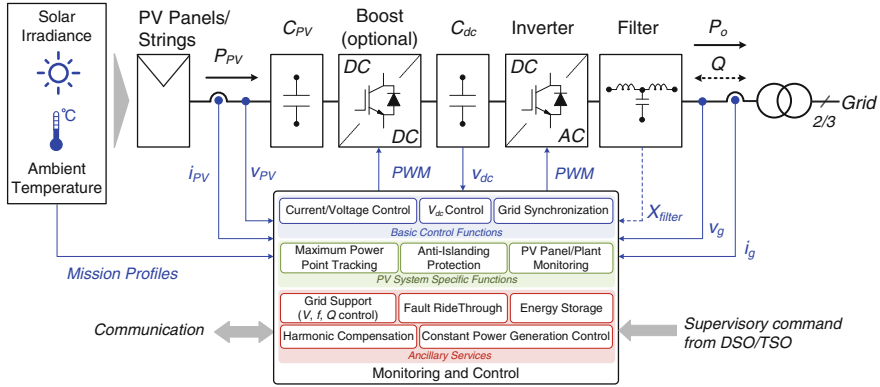


Fig. 9 Hardware schematic and control function blocks of a typical PV system with a DC/DC boost stage

200–600 V) [15, 16]. Moreover, the use of a boost converter offers flexibility to extract maximum power from the PV panels, which is a basic requirement for PV systems and known as Maximum Power Point Tracking (MPPT). There are also other basic requirements for PV systems, which should be complied with during the design and operation, such as power quality issues, grid synchronization and the anti-islanding protection. In order to perform those basic functions for PV systems, an effective monitoring system, which offers the system operation conditions (e.g. grid conditions and mission profiles), is necessary.

2.1.1 Basic Control of Single-Phase Photovoltaic Systems

The control objectives of a single-phase system [3], can be divided into two major parts according to Fig. 9:

- (1) PV-side controller, with the purpose to extract the maximum power from the input source considering mission profiles (ambient temperature and solar irradiance). In general, the protection of the DC/DC converter (boost converter) should also be taken into consideration in this controller.
- (2) Grid-side controller, with the purpose to fulfill the basic requirements. Thus, the grid-side controller can have the following tasks:

- control of the active power delivered to the grid;
- control of the reactive power exchange with the grid;
- high efficiency and high quality of the injected power;
- grid synchronization, and anti-islanding protection.

A conventional control structure for single-phase systems consists of two-cascaded loops as shown in Fig. 10 in order to fulfill the above requirements.

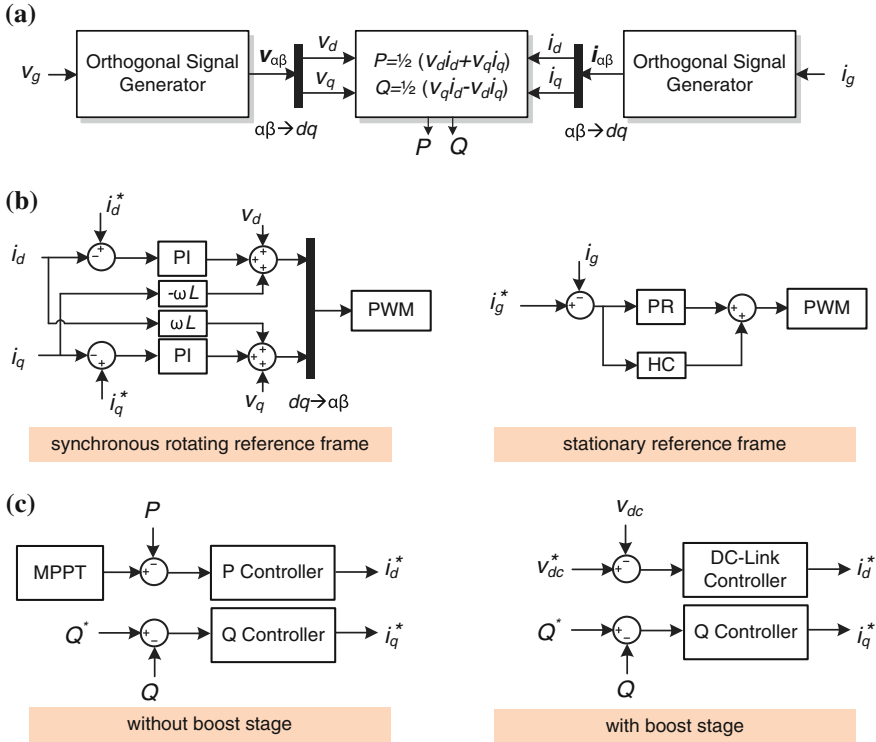


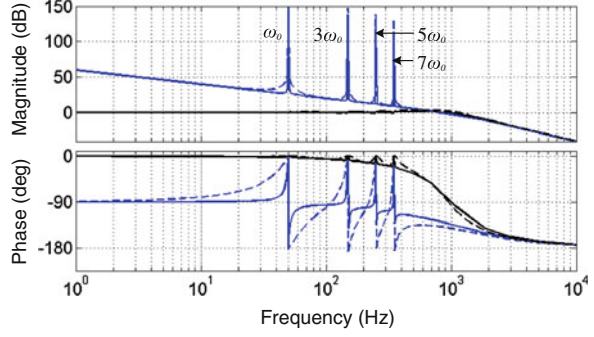
Fig. 10 Conventional single-phase dual-loop control structures with orthogonal signal generators. **a** Power calculation and signal generation. **b** Inner current control loop. **c** Outer control loop for current reference generation

Inner Current Control Loop

For the current control loop, which has the responsibilities of the power quality issues and current protection of the inverter. The existing controllers, such as Proportional Resonant (PR), Resonant Control (RSC), Repetitive Controller (RC), and Deadbeat Controller (DB) can be adopted directly [16–22]. Further, applying a Park transformation ($\alpha\beta \rightarrow dq$) lead to the possibility of Proportional Integral (PI) controllers to regulate the injected current, and afterwards, the modulation reference can be obtained by means of the inverse Park transformation ($dq \rightarrow \alpha\beta$), as it is shown in Fig. 10. Since the current control loop is responsible for the power quality, this responsibility should also be effective and valid in the design of current controllers and the *LCL*-filter. By introducing Harmonic Compensators (HCs) for the controller and adding passive damping for the filter, an enhancement of the current controller tracking performance can be achieved and the background distortion influence is alleviated [3, 16, 17, 20, 22].

The PR controller with Harmonic Compensators (PR + HC) presents a good performance in terms of accurate tracking and fast dynamic response compared to the PI controller [22]. The transfer function of this controller can be given as,

Fig. 11 Open loop (blue) and closed loop (black) Bode diagrams of the PR current controller with different sets of k_{rh} : $k_p = 22$, $k_r = k_{rh} = 500$ (solid line) and $k_r = k_{rh} = 5,000$ (dashed line), where $h = 3, 5, 7$



$$G_i(s) = k_p + k_r \frac{s}{s^2 + \omega_0^2} + \sum_{h=3,5,7,\dots} \frac{k_{rh}s}{s^2 + (h\omega_0)^2} \quad (1)$$

where k_p is the proportional gain, k_r is the fundamental resonant control gain, k_{rh} is the control gain for h -order resonant controller and ω_0 is the grid fundamental frequency. As it is shown in Fig. 11, the cascaded HCs can effectively suppress the harmonics at the corresponding resonant points if the gains are high enough.

Outer Control Loop for Current Reference Generation

The outer voltage/power control loop shown in Fig. 10 provides the system operation conditions (e.g. grid voltage amplitude and grid frequency) and then it generates a current reference, which is subsequently utilized in the inner current control loop. Thus, it offers the possibilities to add control methods into this loop to shape the injected grid current. For example, based on the single-phase PQ theory [21, 22], the injected grid current reference can be produced by regulating the averaged active power and reactive power, as it is shown in Fig. 10. This power control method is intuitive and simple, since the averaged active power and the averaged reactive power references (P^* and Q^*) can directly be set by the operators. With the help of orthogonal signal generator systems (e.g. Hilbert transform) [21], the grid current reference i_g^* can be expressed as,

$$i_g^* = \frac{1}{v_\alpha^2 + v_\beta^2} \begin{bmatrix} v_\alpha & v_\beta \end{bmatrix} \begin{bmatrix} G_P(s)(P - P^*) \\ G_Q(s)(Q - Q^*) \end{bmatrix} \quad (2)$$

where v_α, v_β are the orthogonal components of the grid voltage, respectively, P, Q are the averaged active power and reactive power, P^*, Q^* are the power references and $G_P(s), G_Q(s)$ are PI-based controllers for the active power and the reactive power, respectively. The grid current is then controlled as shown in Fig. 10.

There are also other control possibilities available for the outer control loop of a single-phase system, such as the droop-based control and the instantaneous power control [18, 21]. The droop-based power control method is implemented based on the assumption that the distributed line is mainly inductive [21]. However, in fact, the PV systems have been dominated by residential applications with low rated

power and low voltage grid. In the case of those applications, such assumption is not valid. The instantaneous power control method acts directly on the instantaneous power, and subsequently the reference current is produced. Thus, there is no need to calculate the averaged active power and reactive power for this method [18]. Nevertheless, in respects to the control of grid-connected PV systems, the basic requirements imposed by the Distributed System Operators (DSOs) and/or national committees should be followed as exactly as possible.

Grid Synchronization

The injected current into the grid has to be synchronized with the grid voltage as the standards in the field [3]. Therefore, grid synchronization algorithms play an important role for the PV systems. Moreover, in respect to the above control methods, e.g. the *PQ* control strategies, a fast and accurate synchronization system will strongly contribute to the dynamic performance and the stability margin of the whole control systems. Even for the instantaneous power control method, the syntheses of instantaneous power reference from the averaged active power and reactive power references is affected by the knowledge of the grid conditions.

Different methods to extract the phase angle have been developed and presented in many studies. Here is presented a brief description of the main methods:

- *Zero-Crossing Method*, which has the simplest implementation. However, due to the poor performances mainly when grid voltages register variations such as harmonics, it is not the optimal synchronization method.
- *Filtering of Grid Voltage*, being another possibility to extract the phase angle. With dedicated orthogonal signal generator systems, improved performance of the zero-crossing method in single-phase applications is achieved, but still, the filtering method encounters difficulty when the grid presents variations.
- *Phase Locked Loop (PLL) Technique*, has been the state-of-the-art method to detect the phase angle of the grid voltage [3, 16, 21]. This algorithm has a better rejection of grid harmonics, notches, and any other kind of disturbances. However, for single-phase applications, focuses should be paid on the creation of the orthogonal signal generator systems.

Grid Condition Monitoring (Fault Detection)

Grid condition information is very important for the control system to perform special functionalities. The voltage sag detection is the way to identify a voltage fault and it determines the dynamic performance of the voltage sag compensator for the distributed systems and the behavior of the whole control system [22–24]. For single-phase system, the Root Mean Square (RMS) method, peak value method (OSG based sag detection techniques), the missing voltage technique and wavelet transform method [22, 23] can be used to monitor the grid voltage and detect the fault.

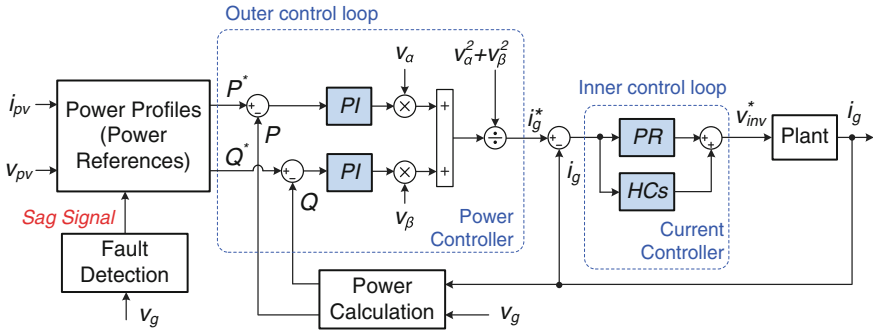


Fig. 12 Dual-loop control system of a single-phase single-stage PV system with low voltage ride through capability based on the single-phase PQ theory and PR + HC current controller

2.1.2 Advanced Control of Single-Phase PV Systems Under Grid Faults

In the case of a wide-scale penetration of single-phase PV systems in the distributed grid, the disconnection due to unintentional anti-islanding protection under grid faults can contribute to: (a) voltage flickers, (b) power outages, and (c) system instability [4, 5, 21]. In order to address those issues, the current active grid codes are suggested to be modified for the PV systems with ancillary services. Some grid standards have been updated already. The next generation PV systems should be capable to ride-through low voltage and provide reactive power to support the grid at the same time. The performance of such systems under grid faults can be enhanced by a better voltage sag detection unit in terms of fast response and accuracy. Referring to Fig. 10, an intuitive and easy way for a single-phase PV system to inject reactive power during grid faults is based on the single-phase PQ theory, as it is shown in Fig. 12, including a fault detection unit.

The “Power Profiles” unit in Fig. 12 is used to generate the average active power and reactive power references for the power controllers, and subsequently, the references are regulated to produce the grid current reference. In the normal operation mode, the average active power reference P^* is the output of a MPPT system and the whole system is required to operate at unity power factor to deliver as much energy as possible to the grid. When a grid voltage fault is detected by the “Fault Detection” unit, the PV system enters into the LVRT operation mode. According to the grid requirements defined in Fig. 2b, three major possibilities are available for single-phase PV systems to inject reactive power [5, 23].

Constant Peak Current Strategy

With this control strategy, there is no risk of inverter shutdown due to overcurrent protection, as the amplitude of the injected grid current (I_{gmax}) is kept constant during the voltage sag. The injected reactive current level (I_q) is dependent of the voltage level. According to Fig. 2b, the grid peak current I_{gmax} can be set as the rated current level I_N of the PV system, for example,

Fig. 13 Representation of the grid current and the grid voltage of a single-phase PV system with constant peak current control strategy ($v_g \geq 0.5$ p.u.)

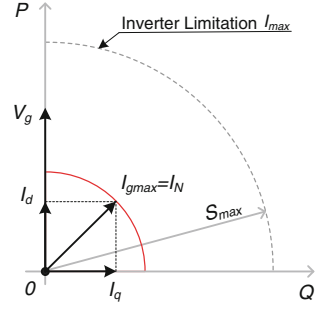
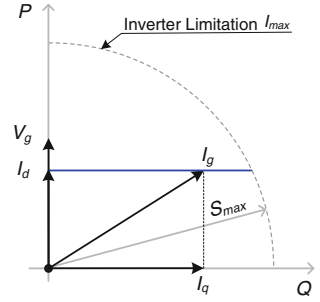


Fig. 14 Representation of the grid current and the grid voltage of a single-phase PV system with constant active current control strategy ($v_g \geq 0.5$ p.u.)



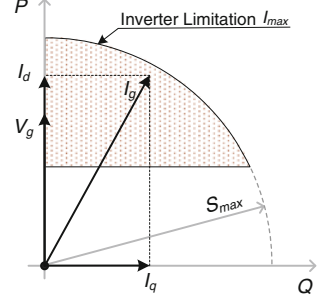
$$\begin{cases} I_{g \max} = I_N \\ I_q = k(1 - v_g)I_N \end{cases} \quad (3)$$

in which v_g is the grid voltage in p.u., $0.5 \text{ p.u.} \leq v_g \leq 0.9 \text{ p.u.}$, and $k \geq 2 \text{ p.u.}$. Based on Fig. 2b, the PV inverter should generate full reactive power ($I_q = I_N$) when $v_g < 0.5 \text{ p.u.}$. The phasor diagram for this control strategy is shown in Fig. 13, from which it can be observed that the output active power decreases ($I_d < I_N$ and $V_g < V_{gn}$) during LVRT.

Constant Active Current Strategy

Another control possibility under LVRT operation is to maintain the active current constant. For the purpose to extract as much energy from the PV panels as possible, the level of active current can be controlled to be that of the rated current ($I_d = I_N$), as it is shown in Fig. 14. The injected reactive current (I_q) is proportional to the voltage sag depth within a voltage range ($0.5 \text{ p.u.} \leq v_g \leq 0.9 \text{ p.u.}$), as it is shown in Fig. 2b. With this reactive power injection strategy, the amplitude of the injected current may exceed the inverter limitation (I_{\max}). To avoid inverter shutdown owing to over-current protection, the following condition should be fulfilled during the design and the operation of a PV inverter,

Fig. 15 Representation of the grid current and the grid voltage of a single-phase PV system with constant average active power control strategy ($v_g \geq 0.5$ p.u.)



$$\sqrt{1 + k^2(1 - v_g)^2} \leq \frac{I_{\max}}{I_N} \quad (4)$$

where v_g is the grid voltage in p.u. and $k \geq 2$ p.u..

Considering a pre-designed inverter with a robustness margin, $I_{\max} = 1.25I_N$, and $k = 2$ p.u., it is not possible to utilize this control strategy to inject the required reactive power, since the minimum margin is 1.41 for $k = 2$ p.u.. In such a case, the PV system should also de-rate the active power output in order to generate sufficient reactive power to support the grid voltage recovery. Otherwise, over-rated operations may introduce failures to the whole system and shorten the inverter serving time, and thus the maintenance cost increases.

Constant Average Active Power Strategy

Similar to the constant active current control strategy, a straightforward way to maximize the output energy (i.e., to deliver maximum active power) is to keep the average active power constant during LVRT, as it is shown in Fig. 15. However, the required injection of reactive power might pose a risk of over-current operation with this control strategy. In case of this, the currents can be expressed as,

$$\begin{cases} I_d = \frac{1}{v_g} I_N \\ I_q = k(1 - v_g) I_N \end{cases} \quad (5)$$

in which v_g and k are defined previously. Thus, the following constraint should be satisfied to avoid inverter shutdown due to over-current protection.

$$\frac{1}{v_g} \sqrt{1 + k^2(v_g - v_g^2)^2} \leq \frac{I_{\max}}{I_N} . \quad (6)$$

In the design and the operation of the PV inverters, those above constraints should be considered. Especially, for the next generation PV systems, the provision of reactive power both in normal operation and under grid faults, and the requirements of LVRT will come into force in the near future. If the above aspects are not well considered, the maintenance costs and energy losses may increase.

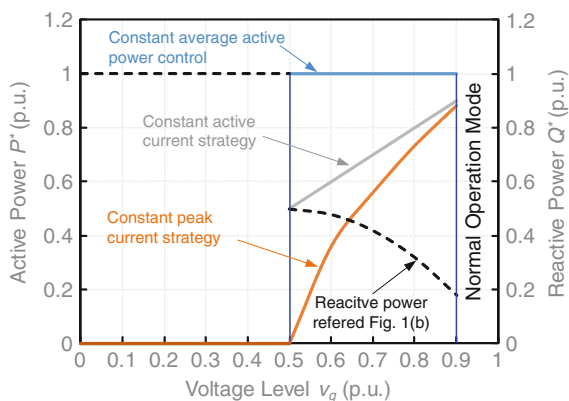


Fig. 16 Reactive power and active power references for a PV inverter under different reactive power injection strategies according to Fig. 2b

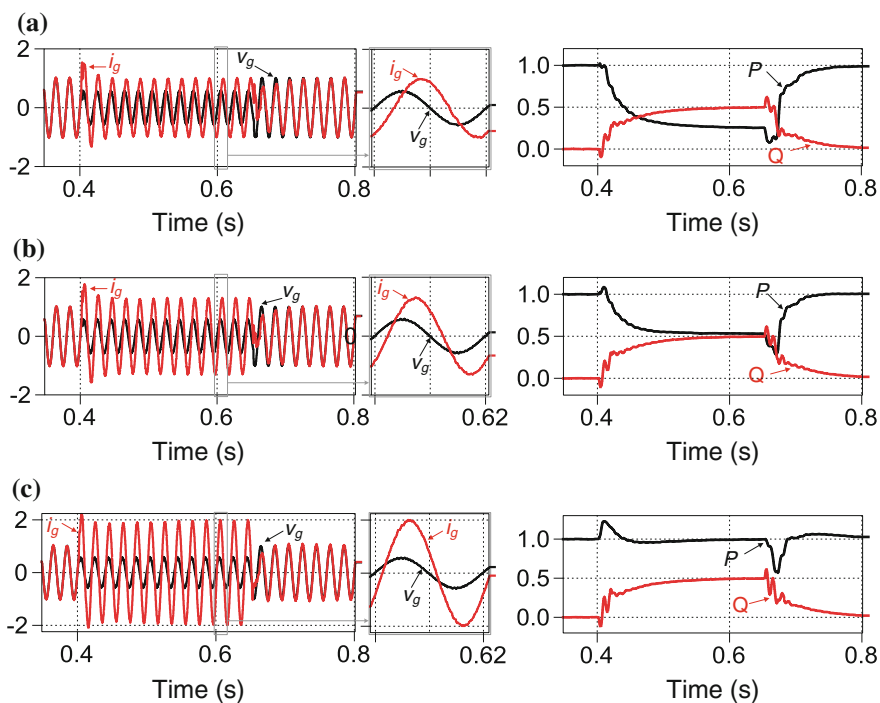


Fig. 17 Simulation results of a single-phase 1 kW PV system in LVRT operation mode with three different reactive power injection strategies: i_g , grid current [p.u.]; v_g , grid voltage [p.u.]; P , average active power [p.u.]; Q , average reactive power [p.u.]; voltage sag level: 0.45 p.u. **a** Constant peak current strategy. **b** Constant active current strategy. **c** Constant average active power strategy

The corresponding active and reactive power under different voltage sag levels for the three reactive power injection strategies discussed above can be given as shown in Fig. 16. Thus, the required reactive power can be injected under different voltage levels according to Figs. 12 and 16. Simulation results of a single-phase PV system in LVRT operation with different reactive power control strategies are given in Fig. 17. The results demonstrate the effectiveness of those reactive power injection strategies for single-phase PV systems.

2.1.3 Constant Power Generation Control of Single-Phase PV Systems

Another issue to cope with for the DSOs is to expand the power infrastructure in order to accept more PV energy in the distributed grid. This challenge is even severe in some countries with an increasing adoption of PV systems, e.g. Germany and Spain [5, 9, 25]. However, the potential cost brought by such line extensions and increased maintenances impose new obstacles. In the light of this, the DSOs are limiting PV installations in order to avoid an extension of the power infrastructure, which is against the goal of the acceptance of more renewable energy resources in those countries. Thus, seen from a total cost perspective, the line extension approach is not the optimal solution to increase PV renewable energy utilizations.

Actually, according to a study of a 3 kW single-phase PV system at a certain place with a yearly mission profile as it is shown in Fig. 18, a 20 % reduction of the maximum feed-in power from PV systems only leads to a limited reduction (6.23 %) of yearly total energy yield. Thus, it is feasible and reasonable to increase PV penetration degree without violating the line capacity by limiting the maximum feed-in power from current existing PV systems. Such issues are already being discussed in some countries where the PV systems share a large electricity generation, e.g. Germany [9]. Thus, the current active PV systems should enter into a Constant Power Generation (CPG) mode when the output reaches a certain level (e.g. 80 % of the peak power) [25, 26, 27]. The cut-off energy can be used in other systems (e.g. energy storage systems), but the total cost will increase. However, the CPG operation control for an individual PV system can be implemented by means of: (a) modifying MPPT control and/or (b) enabling an energy storage system.

With modified MPPT control in the CPG operation mode for an individual PV system, there is no need to install extra devices and thus there are no additional expenses. For a PV system with multi-string inverters connected in parallel, by shutting down a number of string-inverter based PV units, a constant power generation can also be achieved. The flowchart for a PV system with the CPG control by modifying the conventional MPPT algorithm is shown in Fig. 19.

According to Fig. 19, the operation principle is described as following:

When the PV output power P_{pv} exceeds the maximum feed-in power limitation P_{limit} , $P_{pv} > P_{limit}$, the system enters into CPG operation mode and the MPPT control is deactivated. When $P_{pv} \leq P_{limit}$, the system should deliver as much energy as possible to the grid with a MPPT control algorithm, and thus the CPG

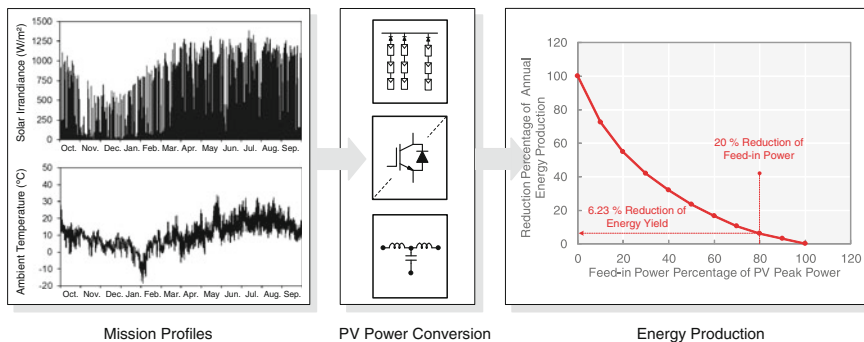
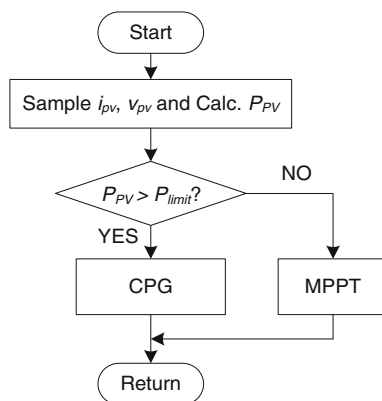


Fig. 18 Energy reduction due to the limitation of maximum feed-in power from a 3 kW single-phase PV system with a yearly mission profiles (Oct. 2011–Sept. 2012) at a certain place in Denmark

Fig. 19 Flowchart of CPG control by modifying MPPT algorithm for a single-phase PV system



control is disabled. During this period, a conventional MPPT algorithm can be adopted, such as the perturb-and-observe and incremental-conductance algorithms.

Study results of a 3 kW single-phase PV system with the CPG control by modifying MPPT algorithm are shown Fig. 20. The study demonstrates the effectiveness of the CPG method by modifying MPPT control. Thus, it is worth to investigate two main issues for the CPG control in order to increase PV penetration level in the future: (a) analyzing the reduction of the energy yield and (b) developing robust CPG control methods. It is also worth to point out that, due to the intermittency, the active power from a large PV system should be constrained to a required value, which is proportional to the possible available power. This control is known as *Delta production control* and is set to avoid imbalances or overloading in the grid in some countries for wind power plants [10]. With the

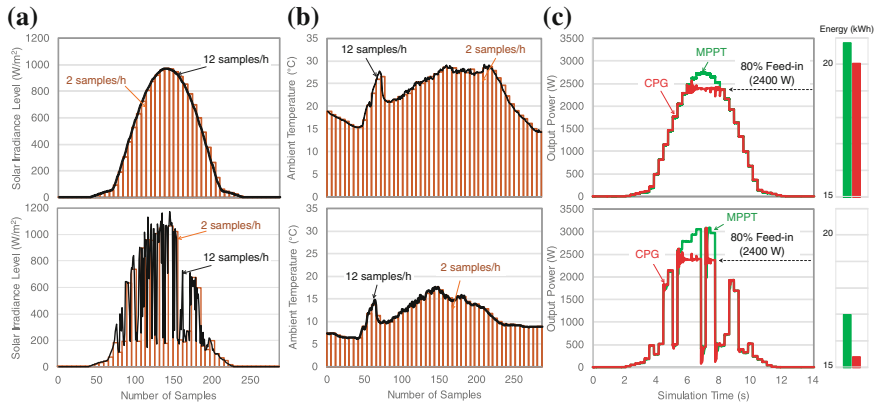


Fig. 20 Output power profiles and energy productions of a 3 kW single-phase PV system with Constant Power Generation (CPG) and MPPT control using measured daily profiles **a** Solar irradiance level (up: clear day, down: cloudy day) **b** Ambient temperature (up: clear day, down: cloudy day) **c** Output power and energy production (up: clear day, down: cloudy day)

same control objectives, such an active power constraint can also be implemented in PV systems, which consist of significantly accumulated small PV units.

2.2 Control of Three-Phase Photovoltaic Systems

Although most of the PV systems are connected to the grid with single-phase converters due to the fact that they are highly used in residential applications, there are also other systems with the same power ratings as those of wind turbine systems. For commercial or industrial purpose, the use of central inverters, ranging from tens to hundreds kilowatts, and up to several megawatts, forms three-phase systems in those applications. Compared to the control of single-phase systems, since there are more control freedoms (grid voltages, grid currents, instantaneous power, etc.), the main control issues of grid-connected three-phase PV converters are transformed through the instantaneous power theory with reference to AC current and voltage controllers [3, 16, 17]. However, since there is an interaction between voltage sequences and current sequences under unbalanced grid faults, which is opt to occur in three-phase systems, either the controlled active power or the controlled reactive power will have oscillations. In other words, the control of three-phase PV systems under grid faults is much more complicated, which will be discussed in the following.

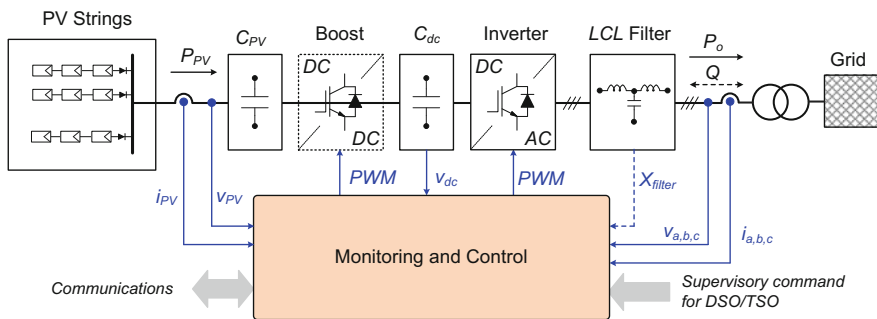


Fig. 21 Hardware schematic and general control structure of a three-phase grid-connected PV system with an *LCL*-filter

2.2.1 Basic Control of Three-Phase PV Systems

Figure 21 shows the general structure of a three-phase PV system with power feed-in functions. The main control features of such a system are similar to those of a single-phase system shown in Fig. 9, such as MPPT control, grid synchronization, reactive power control, and grid supporting features.

The boost stage functions as the input power control stage to extract the maximum power from the PV strings in normal operation. If the input voltage is sufficient for the PV inverter, it might be eliminated but results in the lack of a feasible MPPT control system. The control of the grid-side converter (three-phase PV inverter) is normally implemented by regulating the DC-link voltage in order to maintain the power balance between the PV strings and the grid. It also takes care of the power quality of the generated power by controlling the injected grid current. With the help of the instantaneous power theory and the Clark and Park transformations [3, 16], the synchronization and the control of three-phase PV inverters are easier than that of single-phase PV inverters. The control strategy applied to the three-phase PV inverters more clearly involves two cascaded loops, which have the similar responsibilities as those in single-phase systems. The implementation of the control strategy for such a three-phase PV inverter can be done in different reference frames, such as synchronous rotating (dq -), stationary ($\alpha\beta$ -), and natural (abc -) reference frame [3, 16, 17].

Control Structure in Synchronous Reference Frame

Applying the Park transformation to a three-phase variable (v_{abc} , i_{abc}) leads to the possibility of dq -control for a three-phase system. This control uses the reference frame transformation module ($abc \rightarrow dq$) to transform the grid voltage and current waveforms into a reference frame which rotates synchronously with the grid voltage. Consequently, the control variables are becoming DC quantities. Since every deviation of the grid voltage and/or the grid current will be reflected to the corresponding d - and q -axis components, it leads to an easy solution to filter and control by means of Proportional-Integral (PI) based controllers.

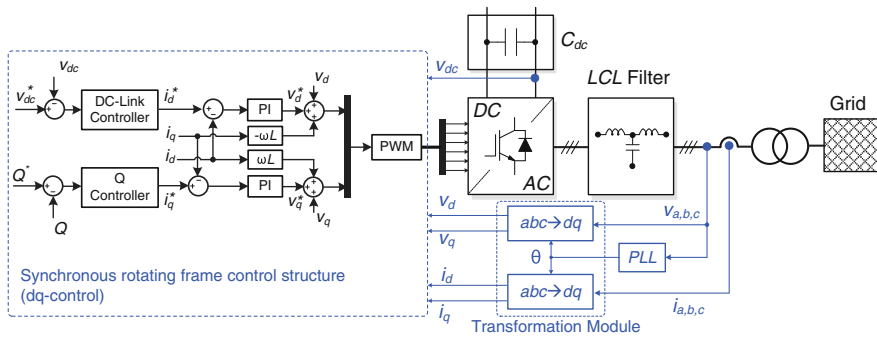


Fig. 22 General control structure of a three-phase PV inverter with synchronous rotating frame control (*dq*-control)

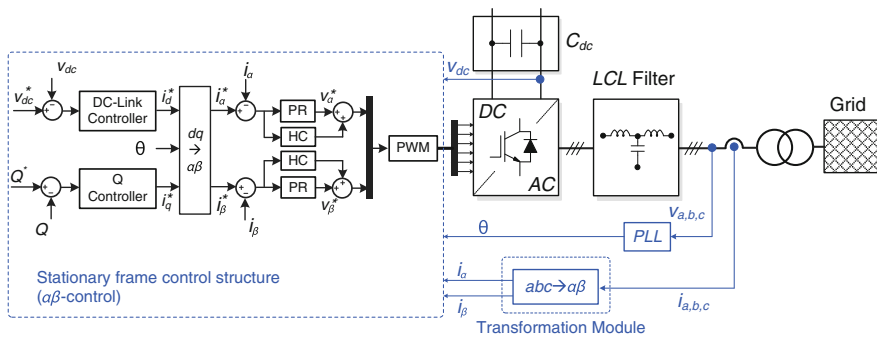


Fig. 23 General structure of a three-phase PV inverter with stationary frame control ($\alpha\beta$ -control)

Figure 22 represents the schematic of the *dq*-control for a three-phase PV inverter. In this structure, the DC-link voltage is controlled in accordance to the necessary output power. Its output is then utilized as the reference for the active current controller, whereas the reactive current reference is usually set to be zero in normal operation. When the reactive power has to be controlled in some cases, a reactive power reference must be imposed to the control system.

Since the grid currents are required to be synchronized with the grid voltage, a Phase-Locked Loop (PLL) system is also included in this control structure. It also provides the grid phase angle, which is necessary for the Park transformation model ($abc \rightarrow dq$). For this control structure, the main drawback is the poor compensation capability of the low-order harmonics in the case of PI based controllers in a grid-connected system, even when cross-coupling terms and voltage feed-forward control are adopted to improve the performance [3, 17, 29].

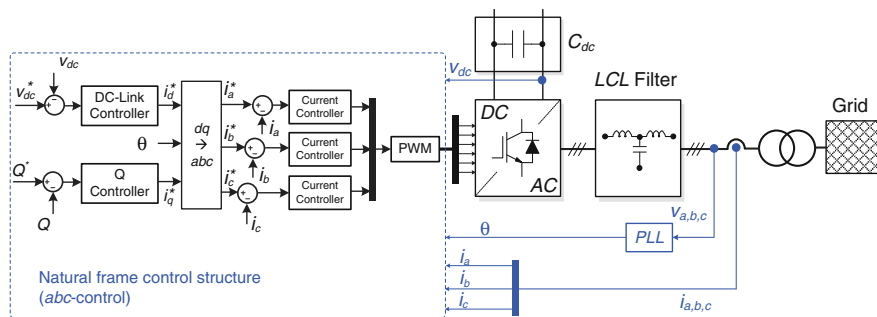


Fig. 24 General structure of a three-phase PV inverter with natural frame control (*abc*-control)

Control Structure in Stationary Reference Frame

Another implementation of the control loops can be done in a stationary reference frame, also known as $\alpha\beta$ -control, which is shown in Fig. 23. In case of this control structure, the control variables (e.g. grid currents) are transformed using the *abc*- $\alpha\beta$ module. The resultant components in the $\alpha\beta$ reference frame are sinusoidal. Since the PI controller is not good at removing the steady-state error when the signal is time varying, employment of other controllers is necessary.

As it is discussed in Sect. 2.1.1 and demonstrated in Fig. 11, the PR controller gained a large popularity due to its capability of eliminating the steady-state error when controlling sinusoidal waveforms, which is the case of $\alpha\beta$ -control. To further improve the injected current quality, Harmonic Compensators (HC) for low-order harmonics (e.g. 3rd, 5th, and 7th order harmonics) can be implemented in parallel with the PR controller, as it is shown Fig. 23. The transfer function of a PR controller with HCs (PR + HC) is represented as (1). Proved in Fig. 11, a low integral time constant k_i or k_{ih} leads to a very narrow resonant band, and thus affecting the performance of the resonant controller. Advanced PR controllers in terms of high dynamic characteristics have also been reported [30].

Control Structure in Natural Reference Frame

In the natural reference control strategy (*abc*-control), an individual controller is applied to each grid current. However, the configurations of the three-phase system structure, e.g. delta, star with or without isolated neutral, etc., pose a challenge for the design of the three individual current controllers. A possible implementation of *abc*-control is shown in Fig. 24 where the DC-link voltage is controlled to generate the active current reference. Then, the current references in *dq*-frame are transformed into three current references using the inverse Park transformation and the phase angle of the grid voltages. Each of the current references is compared with the corresponding measured grid current, and the error goes into the current controller, forming the reference Pulse Width Modulation (PWM) signal for the three-phase PV inverter.

In the case of an *abc*-controlled three-phase PV inverter, three individual current controllers are necessary to create the duty cycles for the PWM pattern, as

it is shown in Fig. 24. The existing controllers, such as PI controller, PR controller, hysteresis controller, dead-beat controller and repetitive controller [3, 17], can be adopted as the three current controllers in the natural reference frame control structure. Selection of those controllers is dependent on the control complexity and its dynamic performance.

2.2.2 Advanced Control of Three-Phase PV Systems Under Grid Faults

As it has been discussed in the previous section, the three-phase instantaneous power theory, the Park transformation and the Clark transformation offer the possibility of feasible control strategies for three-phase PV inverters in normal operations. However, operations under grid faults as required by the TSOs or DSOs increases the control complexity. According to Fig. 5, the grid faults can be classified into two major categories [3]:

- (a) symmetrical/balanced fault is very seldom in the three-phase systems, representing the same amplitude drop on all three grid voltages but no phase shifting;
- (b) asymmetrical/unbalanced fault is when the phases register an unequal amplitude drop together with phase shifting between the faulty voltages. This fault is induced by one or two phases shorted to ground or to each other.

When an asymmetrical fault occurs, the negative-sequence appears in the grid voltages and thus increases the control complexity. In respect to the control strategy under grid faults for three-phase systems, four major possibilities are available. Since the implementation of these strategies gives rise to the injection of unbalanced currents to the grid, specific current control structures, which can properly regulate the positive- and negative-sequence components, are necessary.

Unity Power Factor Control Strategy

One of the control strategies that a three-phase PV system can adopt in the case of grid faults is to maintain a unity power factor during LVRT. According to the instantaneous power theory, the most efficient set of currents, which delivers the instantaneous active power P to the grid, can be given as,

$$\mathbf{i} = g\mathbf{v}, \quad g = \frac{P}{|\mathbf{v}|^2} \quad (7)$$

in which g is the instantaneous conductance and $|\mathbf{v}|$ represents the module of the three-phase voltage vector \mathbf{v} . Under unbalanced grid faults, oscillations at twice the fundamental frequency due to the negative-sequence component will appear in $|\mathbf{v}|$, and thus high-order components will be presented in the injected currents.

It is shown in (7) that the current vector \mathbf{i} is instantaneously proportional to the voltage vector \mathbf{v} . This gives rise to the injection of no reactive power to the grid (unity power factor) since the current vector \mathbf{i} does not have any orthogonal component, which is in relation to the grid voltage. Therefore, in this control

strategy, both active and reactive instantaneous powers are controlled constant during LVRT.

Positive Sequence Control Strategy

The presence of positive-sequence components offers another control strategy for three-phase systems to follow the positive-sequence of the grid voltages. In this case, a better fault detection unit, which can detect the unbalanced grid fault, is necessary. Moreover, the detection system should have high robustness to unbalanced situation and be able to detect the positive sequences of the grid voltages. By this means, the detection of positive- and negative-sequences is the main focus of this control strategy under grid faults.

Since the locked phase angle follows the positive sequence of the grid voltages, the reference currents can be obtained for all control structures for three-phase systems in normal operation, which has been discussed previously, for example, dq -, $\alpha\beta$ -, and abc -control. However, the ripple of the DC-link voltage rises the only problem for this control strategy. This situation can be alleviated by introducing a digital filter. Nonetheless, the DC-link capacitor should be designed with appropriate ratings in order to overcome the second-harmonic ripple presenting during LVRT; otherwise, it may introduce device failures.

With the positive-sequence control, the grid currents will stay sinusoidal and symmetrical during the fault. An increase in amplitude of the grid currents will register due to the amplitude drop of the grid voltages. Since there is an interaction between voltage sequences and current sequences under grid faults, either the controlled active power or the controlled reactive power will present oscillations at twice the grid fundamental frequency during the whole fault period [3, 16, 31]. Thus, in [31], the zero-sequence control path has been introduced in the traditional three-phase system to further increase the control freedoms and to eliminate the oscillations in the controlled power.

Constant Active Power Control Strategy

Another control possibility for three-phase PV systems under grid faults is to maintain the active power constant. In the case of unbalanced grid faults which have been discussed previously, both positive- and negative-sequences will present in the grid voltages, and consequently, leading to unbalanced grid currents. According to the instantaneous power theory, both the active and reactive powers will experience oscillations at twice the grid fundamental frequency due to the unbalanced grid voltages and currents. This gives the rise to the compensation for the double-harmonic components by injecting an amount of negative-sequence in the current reference, which can be expressed as,

$$I^- = -\frac{U^-}{U^+} I^+ \quad (8)$$

where “−” and “+” denote the negative and positive sequence components of both current and voltage.

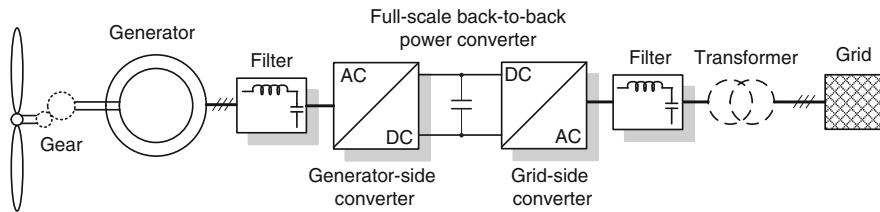


Fig. 25 Basic WTS configuration based on full-scale back-to-back power converters

When this control strategy is applied to a control structure using PI controllers for current regulation, additional controllers for the negative sequence current are needed [3, 16], but the active power can be kept constant during the grid fault. When a control structure based on a PR controller adopts this control strategy, the negative components of the current can be introduced in the current reference since this controller can regulate both positive and negative grid angular frequencies ($+\omega$ and $-\omega$). It is worth to notice that the grid currents are unbalanced during grid faults and that the reactive power presents large oscillations if this control strategy is adopted [3, 31].

Constant Reactive Power Control Strategy

Similar to the case in the constant active power control, an expression can be derived for the reactive power to cancel the double-frequency oscillations. In addition, a current vector, which is orthogonal to the grid voltage vector, can be obtained. Thus, this offers the access to independently control the reactive power if the PV inverters are required to exchange a certain amount of reactive power with the grid. In this case, the reactive power reference is not zero anymore, and it should be set as the desired value according the grid requirements once the grid fault is confirmed.

Consequently, with the above control strategies for three-phase PV systems, the grid codes regarding LVRT under grid faults can be fulfilled. The amount of the injected reactive power should be set depending on the grid requirements imposed by the TSOs or DSOs.

3 Control of Full-Scale Wind Turbine Generation Systems

The full-scale WTS mainly consists of a variable speed controlled generator, which is connected to the grid through a full-scale back-to-back power converter, as it is shown in Fig. 25 [32]. The generator can be an asynchronous generator, an electrically excited synchronous generator (WRSG) or a Permanent Magnet Synchronous Generator (PMSG). The gearbox is not necessary in this case as a heavier direct driven multi-pole generator is adopted. The typical voltage level of the full-scale back-to-back power converter is normally Low-Voltage (LV, below

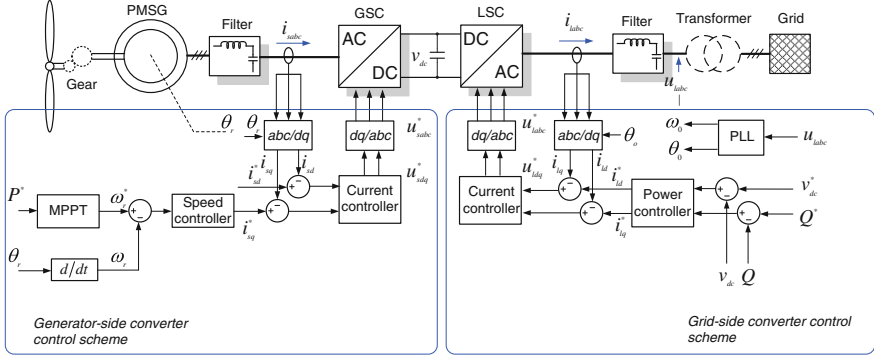


Fig. 26 Control scheme of a PMSG based full-scale back-to-back WTS

1 kV), but systems with Medium-Voltage (MV) level appear also. In the future, the voltage level might be higher so that the system can be connected to the grid without a transformer.

3.1 Basic Control of Full-Scale Back-to-Back WTS

As the full-scale back-to-back power converter works as an interface between the wind power generator and the grid, it must satisfy the requirements of both sides [33–35].

For the Generator Side Converter (GSC) as shown in Fig. 25, the current flowing in the generator stator should be controlled to adjust the generator torque and consequently the rotating speed. This will contribute to the active power balance in normal operation when the maximum power is extracted. The control schemes differ with the generator types. For example, the control structure of a PMSG based full-scale back-to-back WTS is represented in Fig. 26 [35].

When the q -axis is aligned to the rotor magnet flux, the dynamic model for a PMSG based full-scale WTS in dq -reference frames can be described as,

$$\begin{cases} u_{sd} = -R_s i_{sd} - L_s \frac{d}{dt} i_{sd} + L_s \omega_r i_{sq} \\ u_{sq} = -R_s i_{sq} - L_s \frac{d}{dt} i_{sq} + L_s \omega_r i_{sd} + \omega_r \Psi \end{cases} \quad (9)$$

in which, u_{sd} , u_{sq} and i_{sd} , i_{sq} are the stator voltage and current in dq -reference frames, respectively, R_s is the stator resistance and L_s is the stator inductance, and Ψ is the magnet flux. The electromagnetic torque is given as,

$$T_e = \frac{3}{2} p \Psi i_{sq} \quad (10)$$

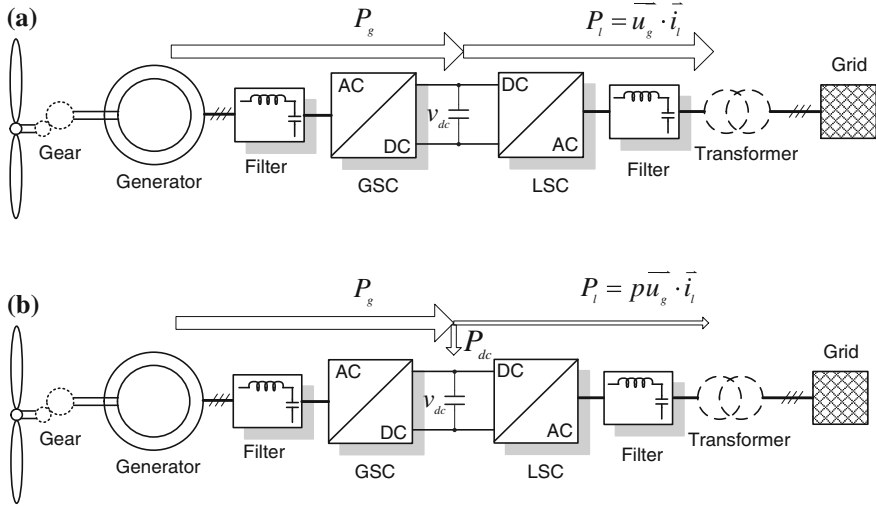


Fig. 27 Power imbalance between the GSC and the LSC of a full-scale back-to-back WTS due to voltage sags. **a** In normal situation. **b** Under grid faults

where p is the pole pairs. It can be concluded from (10) that the torque of the generator, as well as the output active power, can be controlled by controlling the q -axis stator current, as it is shown in Fig. 26.

The control scheme shown in Fig. 26 consists of a speed/power outer loop and a current inner loop. For the GSC, the rotor speed reference ω_r^* is derived from the active power reference P^* controlled by the Maximum Power Point Tracking (MPPT) system. The output of the speed controller is regarded to be the stator q -axis current reference in the inner loop. The output of the inner loop u_{sdq}^* is the voltage reference of the GSC.

For the Line-Side (grid-side) Converter (LSC), it should have the ability to control the DC-link voltage, v_{dc} , in order to ensure that the active power from the GSC can be delivered into the grid. At the same time, the ability of controlling the reactive power is required by the grid codes as well. As shown in Fig. 26, similar to the control of other grid-connected converter, the d -axis is aligned with the grid voltage vector and the DC-link voltage v_{dc} is controlled with the d -axis output current i_{sd} ; while the reactive power Q is controlled by the q -axis current i_{sq} .

3.2 Challenges of Full-Scale WTS Under Grid Faults

In a full-scale WTS shown in Fig. 26, a voltage dip induced by a grid fault has less impact on the generator, since the generator is completely isolated from the grid by the back-to-back converter. However, the power imbalance problem becomes a

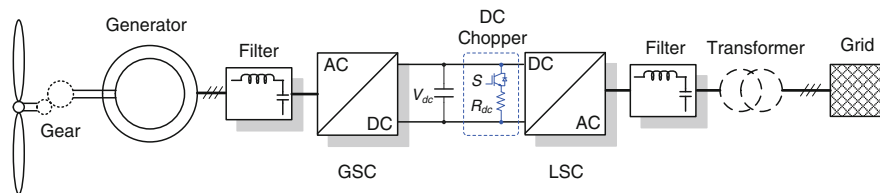


Fig. 28 Full-scale WTS with a DC-chopper for the enhancement of FRT

challenge to the WTS safety. When the grid voltage dip happens, the output active power of the LSC will decrease instantly. Nevertheless, for the generator side, because the generator is connected with the wind turbine, which has a large inertia, the output active power from the generator can only be regulated slowly. Consequently, a power imbalance between the GSC and the LSC will appear, and thus the DC-link voltage may rise, which leads to over-voltage stresses on the switching devices, as it is illustrated by Fig. 27 [36].

For the LSC, the grid voltage dips will introduce power fluctuations and DC-link voltage variations, especially for the unbalanced dips. Its performance under grid faults is similar to that of the three-phase grid-connected PV systems, which has been introduced in Sect. 2.2.

3.3 Advanced Control of Full-Scale WTS in FRT Operation

The main control objectives of a full-scale WTS under grid faults are to balance the power flow between the GSC and the LSC, In order to avoid the DC-link over-voltage, and suppress the power and DC-voltage fluctuations.

3.3.1 FRT of a Full-scale WTS with DC-Choppers

Using a DC-chopper is the simplest way to avoid over-voltage on the DC-link during FRT operation, as it is shown in Fig. 28. When the voltage dip happens and the DC-link voltage v_{dc} rises, the DC-chopper is enabled by switching S , and thus the power from the GSC is dissipated on a series-connected braking resistor R_{dc} . Hence, the energy balance is restored. The braking resistor can also work in the switching mode, and thus the performance of the DC-chopper under different voltage dip levels can be optimized. A pitch control of the wind turbine is another way to limit power from the GSC by directly reducing the input mechanical power, but the response is not fast enough to take away all the power. As a result, it usually works together with a DC-chopper under grid faults in order to enhance the FRT performance [36].

Simulation results of the DC-link voltage in a 2 MW PMSG WTS with a DC-chopper under a 50 % balanced voltage dip is presented in Fig. 29. Compared

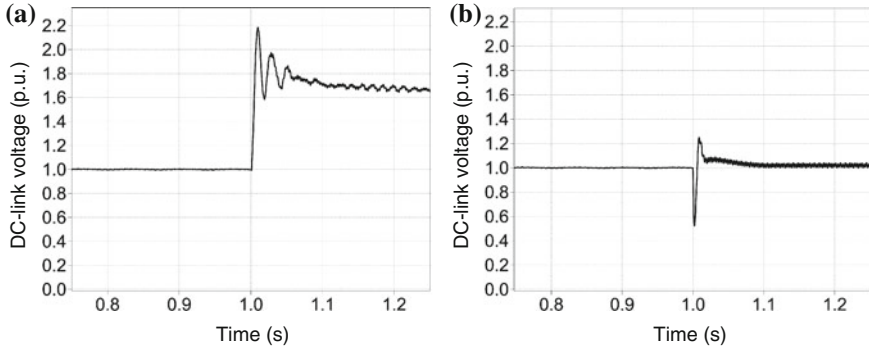


Fig. 29 Performance of a 2 MW PMSG WTS with a DC-chopper in FRT operation mode **a** without a DC-chopper, **b** with a DC-chopper

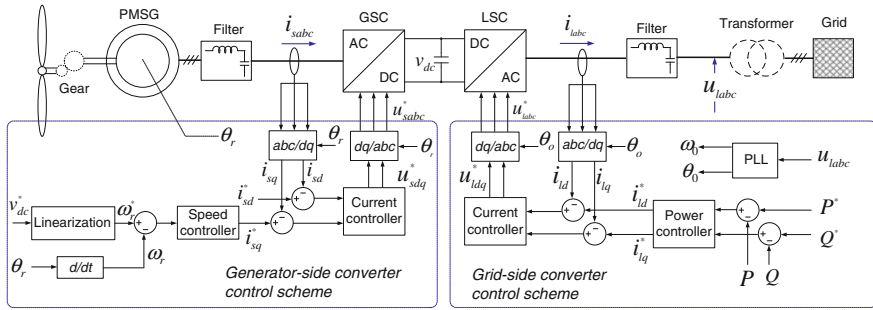


Fig. 30 DC-voltage control scheme of a full-scale PMSG based WTS

with the performance of this system without a DC-chopper in FRT operation, it can be seen that the over-voltage is significant alleviated by the DC-chopper.

3.3.2 DC-Voltage Control of a Full-Scale WTS Under Grid Faults

Another approach to limit the DC-link voltage under grid fault is to use the GSC to control the DC-bus voltage, while the LSC is used to control the output power [37, 38]. The relationship between the DC-voltage v_{dc} and the generator rotor speed ω_r is represented as,

$$C \cdot v_{dc} \cdot \frac{dv_{dc}}{dt} = -J \cdot \omega_r \cdot \frac{d\omega_r}{dt} - P_{load} + \frac{1}{2} \rho \cdot A \cdot C_p(\omega_r) \cdot v_w^3 \quad (11)$$

where C is the DC-link capacitance, J is the system inertia, ρ is the air density, A is the wind turbine swept areas, v_w is the wind speed. $C_p(\omega_r)$ is the power coefficient

of the wind turbine and it is a function of ω_r . Although the relationship is nonlinear because of $C_p(\omega_r)$, the linearization at a given operation point can be achieved with the methods introduced in [37, 38]. After the linearization, the DC-link voltage can be controlled by controlling the rotor speed in the GSC control scheme as it is shown in Fig. 30.

For the GSC, the rotor speed reference is derived from the DC-voltage reference by means of linearization, instead of MPPT control in normal situation, and the rest of the control scheme is similar to that in the normal operation.

For the LSC, the output active power P and reactive power Q is controlled in the outer loop instead of the DC-link voltage. The reactive power support can be achieved by controlling Q . If the LSC still has enough power capacity after the reactive power demand is satisfied, the MPPT control can be applied to generate active power reference P^* . Under unbalanced voltage dips, different control strategies can be applied on the LSC, which are similar to those control strategies for three-phase PV inverters and have also been discussed in Sect. 2.2.2.

3.3.3 LSC Control Under Unbalanced Faults

As for the LSC, the performance under voltage dips is similar to the three-phase PV systems under grid faults. The negative-sequence grid voltage will introduce unbalanced output current, and thus the output active and reactive power and the DC-link voltage will be fluctuated. An advanced control strategy can be used in the LSC. With different current references, desirable control effects can be achieved [16].

4 Control of Doubly-Fed Induction Generators Based Wind Turbine Systems

Although there is a trend to use full-scale power converters in WTS in recent years, the Doubly Fed Induction Generator (DFIG) based WTS with partly scale power converter is still the most widely used variable speed wind turbine until now [34]. The topology is shown in Fig. 31. The stator side of the DFIG is directly connected to the grid, while a partial-scale power converter is responsible for the control of the rotor frequency as well as the rotor speed. The power rating of the partial-scale converter settles the speed range (typically $\pm 30\%$ around the synchronous speed). Moreover, the converter performs as a reactive power compensator and a smooth grid interconnection. Smaller power converters have been the benefits of this concept from economic point of view. However, the main drawbacks are the use of slip rings, some protection schemes, and the controllability under grid faults, which will be discussed in this chapter.

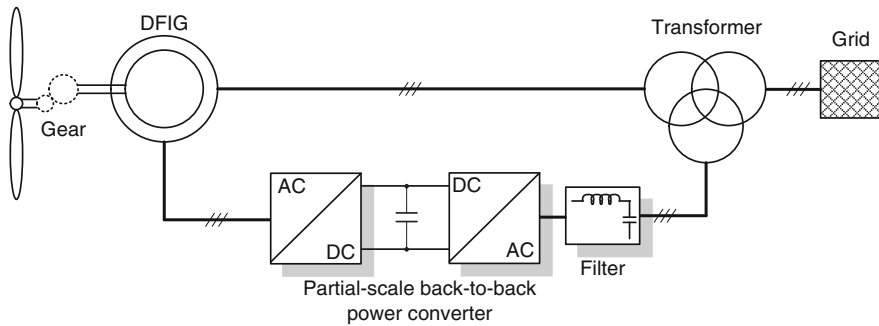
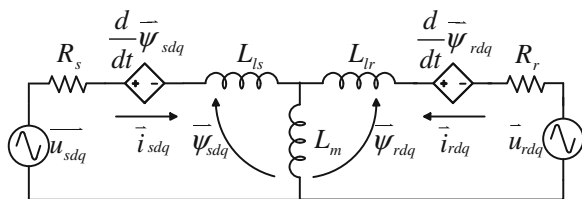


Fig. 31 DFIG based WTS configuration with partial-scale back-to-back power converters

Fig. 32 Equivalent circuit of the DFIG in the dq -reference frame



4.1 Basic Control of DFIG WTS Under Normal Situations

The control of the DFIG is achieved by regulating the partial-scale back-to-back converter. The Rotor Side Converter (RSC) controls the DFIG's rotor speed and power, while the Grid Side Converter (GSC) controls the DC-bus voltage and performs reactive power compensation as well [39].

4.1.1 Control of the Rotor Side Converter

Vector control is one of the most widely used control schemes for the DFIG based WTS. The dq -reference frames in a vector control can be aligned either to the grid voltage or to the stator flux. The dynamic model of the DFIG under grid voltage oriented dq -reference frames can be expressed as,

$$\begin{cases} \bar{u}_{sdq} = R_s \bar{i}_{sdq} + \frac{d}{dt} \bar{\psi}_{sdq} + j\omega_0 \bar{\psi}_{sdq} \\ \bar{u}_{rdq} = R_r \bar{i}_{rdq} + \frac{d}{dt} \bar{\psi}_{rdq} + j\omega_s \bar{\psi}_{rdq} \end{cases} \quad (12)$$

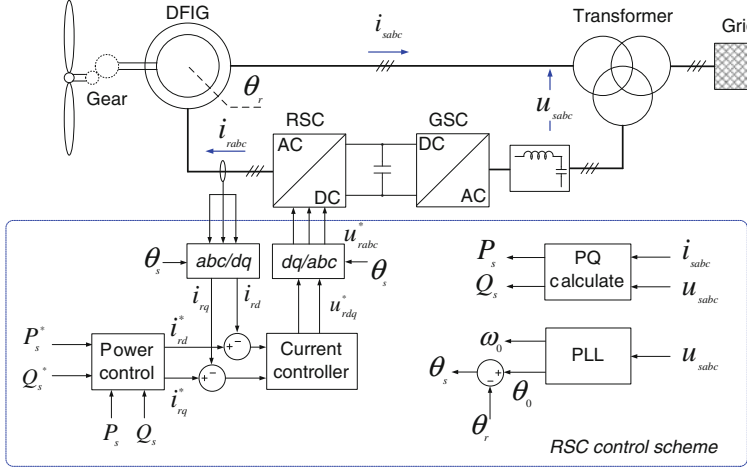


Fig. 33 Voltage oriented vector control scheme for the RSC of a DFIG based WTS

$$\begin{cases} \bar{\psi}_{sdq} = L_s \bar{i}_{sdq} + L_m \bar{i}_{rdq} \\ \bar{\psi}_{rdq} = L_r \bar{i}_{rdq} + L_m \bar{i}_{sdq} \end{cases} \quad (13)$$

where $\bar{u}_{sdq} = u_{sd} + ju_{sq}$ and $\bar{u}_{rdq} = u_{rd} + ju_{rq}$ are the stator and rotor voltages, \bar{i}_{sdq} and \bar{i}_{rdq} are the stator and rotor currents, $\bar{\psi}_{sdq}$ and $\bar{\psi}_{rdq}$ are the stator and rotor flux linkage, respectively, L_m , L_s , and L_r are the magnetizing inductance, stator inductance and rotor inductance, R_s , and R_r are the stator and rotor resistances, respectively. Since the d -axis is aligned with stator (grid) voltage vector, the following is valid,

$$u_{sd} = U_g \text{ and } u_{sq} = 0. \quad (14)$$

Based on (12) and (13), a T-shaped equivalent circuit of the DFIG can be obtained, as it is shown in Fig. 32 where L_{ls} and L_{lr} are the stator and rotor leakage inductances and $L_s = L_m + L_{ls}$, $L_r = L_m + L_{lr}$.

The active power and reactive power output from the stator side of DFIG can be derived from (12) and (13), and can be expressed as (15). It can be concluded that the stator output active power is related to the rotor d -axis current and the reactive power is related to the rotor q -axis current only. As a result, the active and reactive power can be adjusted separately by controlling the rotor dq currents. The grid voltage-oriented vector control scheme for the RSC of the DFIG is shown in Fig. 33, which consists of a inner current loop and a outer power loop. PI controllers are typically used in the inner loop to regulate the dq currents, whereas the PR controllers can be used to enhance the control performance under distorted grid voltages [3].

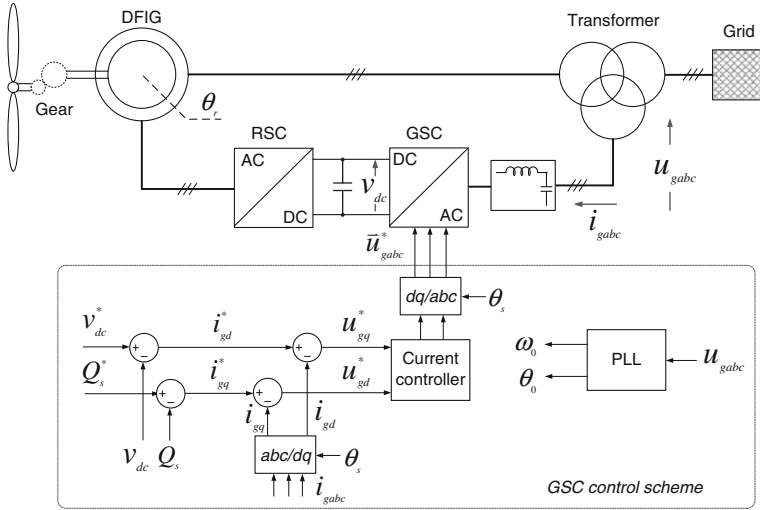


Fig. 34 Control scheme for the GSC of a DFIG based WTS

$$\begin{cases} P_s = -U_g \frac{L_m}{L_s} \cdot i_{rd} \\ Q_s = U_g \frac{L_m}{L_s} \cdot i_{rq} + \frac{U_g^2}{\omega_1 L_s} \end{cases} \quad (15)$$

4.1.2 Control of the Grid Side Converter

The control scheme of the GSC in a DFIG WTS is similar to that in a full-scale back-to-back WTS. As it is shown in Fig. 34, the GSC is controlled by regulating the DC-link voltage and the reactive power.

4.2 Challenges of the DFIG WTS Under Grid Faults

The main drawback of the DFIG WTS is its poor controllability under grid faults. As the stator of the DFIG is directly connected to the grid, the voltage dips induced by the grid faults, either balanced or unbalanced, will normally generate a natural flux, which stand still with the stator windings, resulting in large voltage and current transients. Furthermore, under unbalanced dips, a negative sequence component will also appear which makes the situation even worse [40–43].

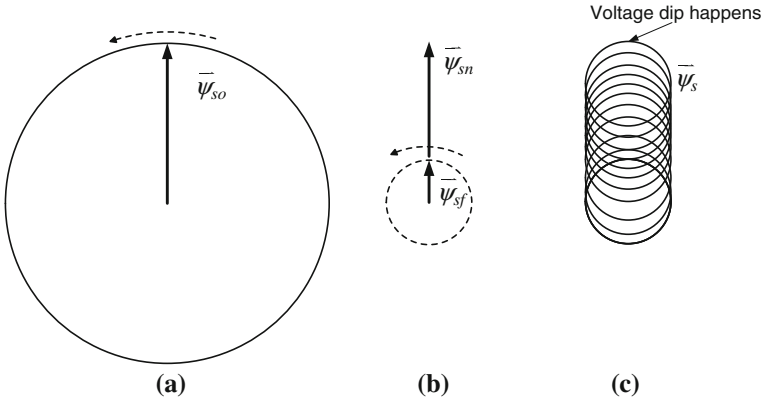


Fig. 35 Trajectory of the stator flux in the DFIG during a 80 % voltage dip: **a** before the voltage dip, **b** at the dip moment, **c** after the voltage dip

Fig. 36 The stator dq-flux of DFIG after a 50 % voltage dip

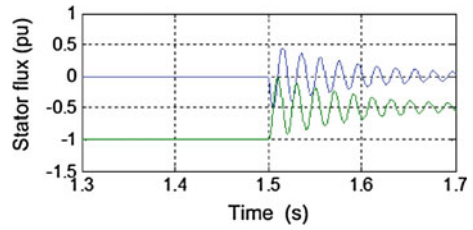
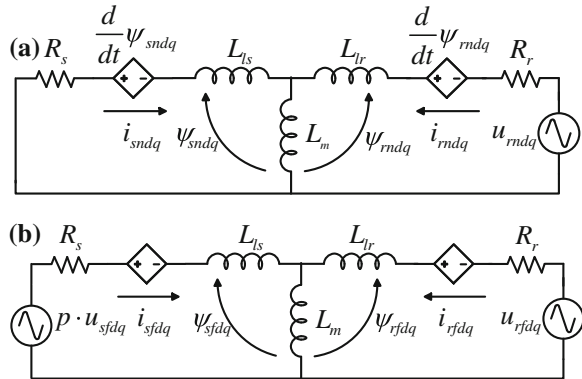


Fig. 37 Equivalent circuits of the DFIG during voltage dips: **a** the natural machine and **b** the forced machine



4.2.1 Performance of the DFIG Under Symmetrical Grid Faults

The symmetrical grid faults will normally introduce balanced voltage dips at the terminal of a DFIG WTS. The stator voltage drops instantly when a grid fault happens. According to the flux conservation principle, the stator flux cannot change

at the speed of stator voltage drop, and thus a natural flux $\bar{\psi}_{sdq}$ will hereby appear, which can be expressed as,

$$\bar{\psi}_{sn} = \frac{p \cdot \bar{u}_s}{j\omega_0} \quad (16)$$

where p is the voltage dip level.

Consequently, the stator flux after the voltage dips is the sum of two components with different frequencies. One is the stator natural flux ($\bar{\psi}_{sn}$) produced by the voltage dips, which is a DC component in the stator static reference frame, and the other is the stator forced flux ($\bar{\psi}_{sf}$) produced by the remaining grid voltage, which is rotating with the grid voltage vector and with the grid frequency. The trajectory of the stator flux after a 80 % voltage dips is shown in Fig. 35, and the stator flux in dq -reference frame is shown in Fig. 36.

According to the superposition principle, the dynamic model of DFIG under balanced voltage dips can be described with two independent equivalent circuits.

(a) The natural machine is short-circuited while the natural flux $\bar{\psi}_{sn}$ exists in the stator winding, and (b) the forced machine is the remaining grid voltage and no transient flux exists [42]. The natural and forced machine in dq reference frame is shown in Fig. 37. Where $\bar{\psi}_{sndq}$, $\bar{\psi}_{rmdq}$, $\bar{\psi}_{sfdq}$ and $\bar{\psi}_{rfdq}$ are the stator and rotor flux in the natural and forced machine, respectively and $\bar{\psi}_{sndq} = \psi_{snd} + \psi_{snq} \cdot \bar{i}_{sndq}$, \bar{i}_{rmdq} , \bar{i}_{sfdq} and \bar{i}_{rfdq} are the stator and rotor current in the natural and forced machine, respectively. \bar{u}_{rmdq} , \bar{u}_{sfdq} and \bar{u}_{rfdq} are the rotor voltage in the natural machine and stator, rotor voltage in the forced machine, respectively.

The rotor Electro-Motive Force (EMF) in the natural machine and forced machine can be expressed as (17) and (18), respectively.

$$\bar{e}_m \approx -\frac{L_m}{L_s} j\omega_r e^{-\frac{t}{\tau_s}} \bar{\psi}_{sn} \quad (17)$$

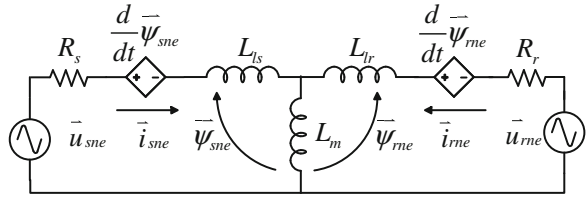
$$\bar{e}_{rf} \approx -\frac{L_m}{L_s} j\omega_s \bar{\psi}_{sf} \quad (18)$$

where τ_s is the damping time constant of the stator natural flux, if the rotor is open-circuited for the natural machine,

$$\tau_s = \frac{L_s}{R_s} \quad (19)$$

As the DFIG usually operates under the rotor speed around synchronous speed (0.7–1.2 p.u.), the rotor speed ω_r is much larger than the slip speed ω_s . As a result, the EMF produced by the stator natural flux will be much larger than the rotor EMF in the normal situations, which may result in large transient current in rotor and destroy the RSC.

Fig. 38 Equivalent negative machine model of the DFIG



4.2.2 Performance of the DFIG Under Asymmetrical Grid Faults

During asymmetrical grid faults, unbalanced voltage dips will be introduced at the terminal of the WTS, and be companied with phase jumps in some cases.

Besides of the stator natural and forced flux, a stator negative flux will also be introduced by the negative-sequence grid voltage. Another equivalent circuit—the negative machine, can be used to analyze the performance of DFIG, together with the natural machine and the forced machine [43]. The equivalent model is shown in Fig. 38.

The stator voltage in the negative machine is the negative-sequence grid voltage, and the rotor EMF produced by the negative-sequence stator flux is represented in (20). Compared to (17) and (18), it can be concluded that the rotor EMF produced by the stator flux with the same amplitude in the negative machine is much larger than that in the forced machine, and even larger than that in the natural machine.

$$\bar{e}_{rne} \approx \frac{L_m}{L_s} j(\omega_0 + \omega_r) \bar{\psi}_{sne} \quad (20)$$

With the existing of the forced flux and the negative-sequence flux, the steady-state stator flux trajectory after asymmetrical grid fault will be an ellipse. The stator flux trajectory under a single phase to ground fault is shown in Fig. 39a.

The stator natural flux produced during the asymmetrical grid faults not only depends on the fault types and voltage dip levels, but also depends on the time when the fault happens. If the fault happens at $t = T_0$ when the positive and negative-sequence grid voltage have the opposite directions, the sum of stator forced and negative flux after fault will be the same as the stator flux before the fault, and thus the stator natural flux will be zero, it is shown in Fig. 39b. When the fault happens at $t = T_0 + \pi/2$, the stator natural flux will be maximum, as it is shown in Fig. 39c, and in this case, it can be given as,

$$\bar{\psi}_{sn}|_{t=T_0+\frac{\pi}{2}} = \frac{2}{3} p \cdot \frac{\bar{u}_s}{j\omega_0} \quad (21)$$

The rotor EMF produced by the natural machine can be calculated by (17) as well. Under asymmetrical grid fault, the RSC has to deal with not only the natural and forced rotor EMF, but also the negative-sequence EMF. The RSC may be saturated under serious voltage dips.

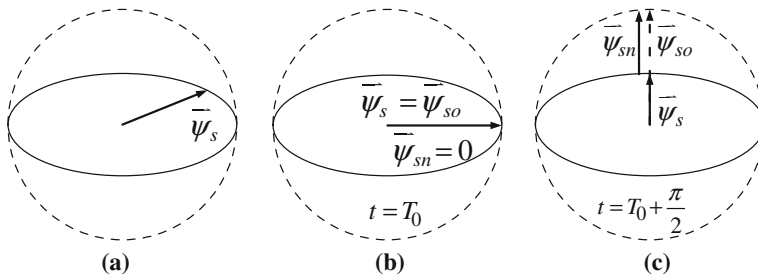


Fig. 39 Trajectory of the stator flux during asymmetrical grid faults: **a** the steady state after faults, **b** the situation with zero natural flux and **c** the situation with the maximal natural flux

Fig. 40 Grid voltage during a recurring grid fault, from the recovery of the first grid fault until the next grid fault happens

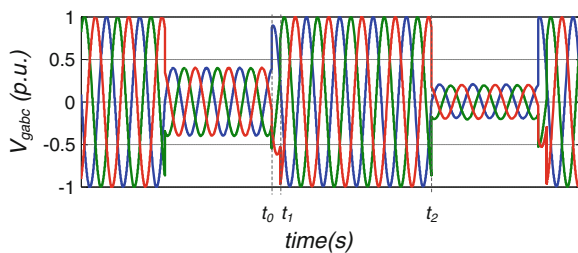


Table 2 Stator natural flux produced by the voltage recovery

θ	85°	75°	60°	45°
$\vec{\psi}_{sdqn} _{t=t_3}$	$0.124 \cdot \frac{P \cdot \vec{u}_{sdq}}{j\omega_0}$	$0.366 \cdot \frac{P \cdot \vec{u}_{sdq}}{j\omega_0}$	$0.707 \cdot \frac{P \cdot \vec{u}_{sdq}}{j\omega_0}$	$\frac{P \cdot \vec{u}_{sdq}}{j\omega_0}$

4.2.3 Performance of the DFIG Under Recurring Grid Faults

The new grid codes in some counties (e.g. Denmark) demand the WTS to ride through multiple grid faults which are happening within a certain time range, also known as recurring faults immunity. An example of two three-phase symmetrical recurring faults is shown in Fig. 40. These recurring faults last for 100 ms from the recovery of the first grid fault to the next one.

The performance of the DFIG during the first voltage dip will be the same as that in the single voltage fault. The analysis started at $t = t_0$ when the grid voltage starts recovering. The recovery of the three-phase voltage will take place gradually in most cases, as the breakers in power systems can only open at the current zero-crossing points. The grid voltage comes back to normal conditions at $t = t_1$. During t_0 and t_1 , the three-phase symmetrical fault will become a two-phase asymmetrical fault, and this period lasts for 5 ms normally.

After t_1 , the grid voltage reaches the normal condition, but a natural flux will be introduced, similar to the case of voltage dips. However, the natural flux produced

by the voltage recovery is normally smaller than that under voltage dips, depending on the angle between fault current and voltage (θ), as shown in Table 2. Moreover, since the grid voltage is normal after the grid recovery, the torque and the power fluctuations brought by the natural current with the same amplitude will be larger than that under voltage dips.

The next grid fault happens at $t = t_2$. If the natural flux produced by the voltage recovery has been decayed before t_2 , the performance of the DFIG under the next voltage dip will be the same as that under a single voltage dip. However, if the natural flux produced by the voltage recovery still exists at t_2 , it may be superposed on the natural flux produced by the next voltage dip, as it is shown in (22).

$$\bar{\psi}_{sn}|_{t=t_2} = \bar{\psi}_{sn_r} + \bar{\psi}_{sn_d} \quad (22)$$

in which $\bar{\psi}_{sn_r}$ is the remaining natural flux when the next voltage dip comes and $\bar{\psi}_{sn_d}$ is the natural flux produced by the next voltage dip. If this happens, the stator natural flux after the second grid fault may be larger than that in single dips, which will normally result in large transient current and voltage on the rotor side.

4.3 Advanced Control of the DFIG WTS in FRT Operation

The FRT of the DFIG WTS can be achieved by applying the advanced control strategies to the RSC. However, since the rotor EMF produced by the stator natural and negative flux is higher than that in normal situation, the RSC may be saturated when the voltage dip level is high. In that case, a breaking chopper is required on the DC-link in order to prevent the over-voltage.

The advanced control strategies for the DFIG WTS under grid faults aim at accelerating the damping of the natural flux as well as limiting the rotor current. Nonetheless, normally, a trade-off has to be made between the two control objectives. Two advanced control strategies are introduced in this section. One is the demagnetizing current control, which focuses on accelerating the damping of natural flux, and the other is the stator and rotor current control, which aims at limiting the stator and rotor current.

4.3.1 Demagnetizing Current Control

The demagnetizing current control proposed by D. Xiang et al. [44, 45] uses the rotor current to accelerate the damping of the stator natural flux. The relationship between rotor natural current and stator natural flux in the natural machine can be derived from (12), (13) and Fig. 37a. It can be given as,

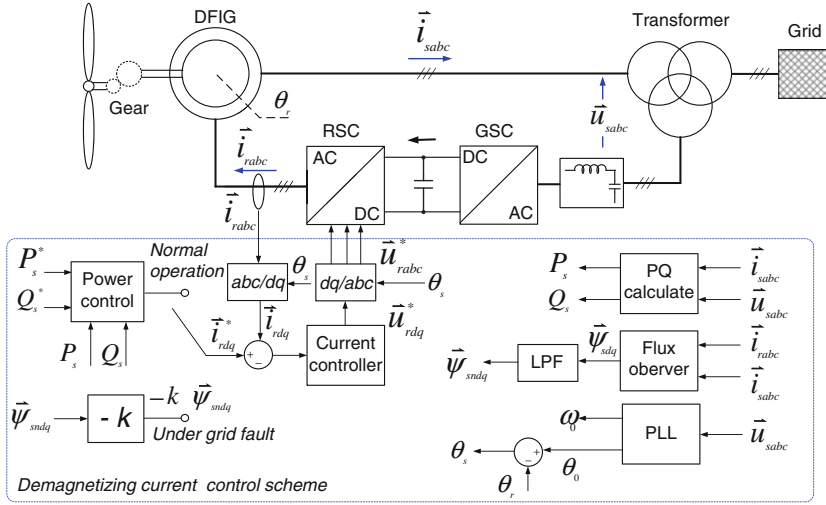


Fig. 41 Control scheme of demagnetizing control for a DFIG WTS

$$\frac{d}{dt} \bar{\psi}_{sn} = -\frac{R_s}{L_s} \bar{\psi}_{sn} + \frac{L_m}{L_s} R_s \bar{i}_{rm}. \quad (23)$$

From (23), it can be concluded that if the rotor current \bar{i}_{rm} is in the opposite direction with the stator natural flux $\bar{\psi}_{sn}$ as shown in (24), the damping of $\bar{\psi}_{sn}$ will be accelerated. The demagnetizing control is set based on (24), with the control scheme shown in Fig. 41.

$$\bar{i}_{rm} = -k\bar{\psi}_{sn} \quad (24)$$

The stator flux in the dq -reference frame $\bar{\psi}_{sdq}$ is obtained from the flux observer; the stator natural flux in dq -reference frame is with the frequency of ω_0 , while the forced flux is the DC-component. Therefore, the stator natural flux $\bar{\psi}_{sdq}$ can be separated through a Low Pass Filter (LPF). Under grid faults, the current reference is calculated based on (24) and the damping of the stator flux will be accelerated. Noticed that the larger the rotor demagnetizing current is, the faster the damping of stator natural flux becomes. A simulation in a 1.5 MW DFIG WTS under a 50 % symmetrical voltage dip is shown in Fig. 42. The parameters of the DFIG used in the simulations are listed in Table 3. Compared with the normal vector control, it can be seen how the damping of the stator flux is accelerated. However, in order to achieve better damping performance on the stator natural flux, a large rotor current cannot be avoided. At the same time, the demagnetizing current may introduce torque fluctuations with the stator flux, as shown in Fig. 42a.

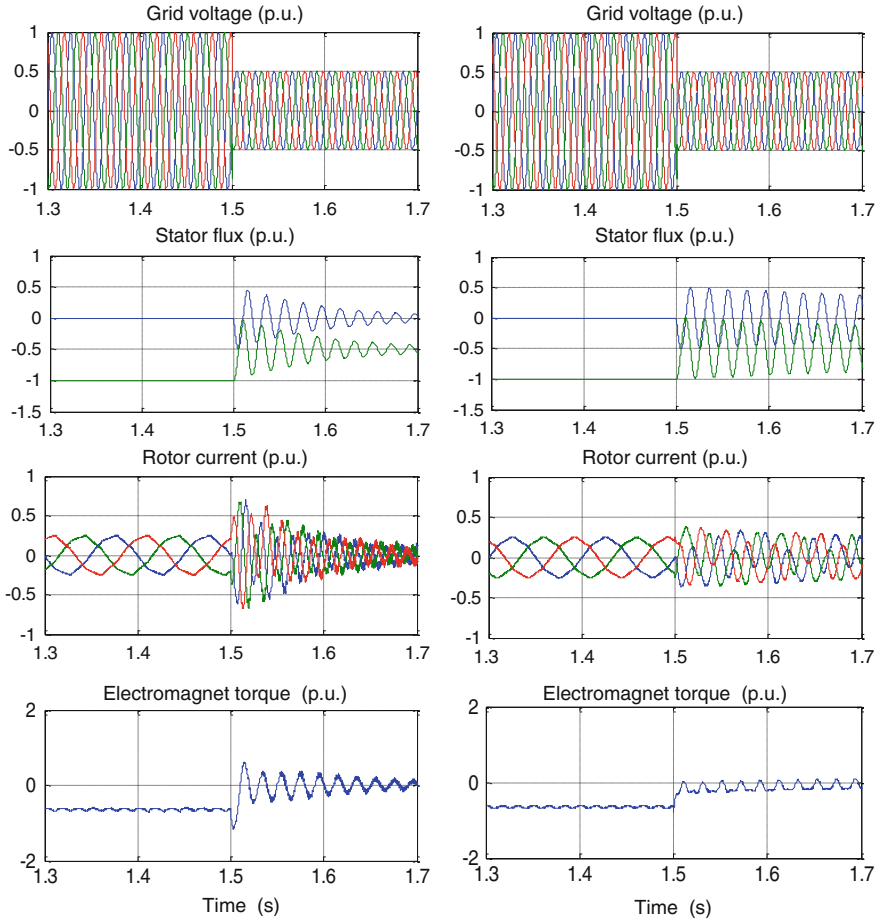


Fig. 42 Simulation results of a 1.5 MW DFIG WTS under 50 % symmetrical voltage dips: **a** with demagnetizing current control and **b** with normal vector control

Table 3 Parameters of the 1.5 MW DFIG used in the simulations

Rated power	1.5 MW	Mutual inductance L_m	4.00 mH
Rated line-to-line voltage	690 V	Stator inductance L_s	4.05 mH
Stator resistance R_s	2.139 m Ω	Rotor inductance L_r	4.09 mH
Rotor resistance R_r	2.139 m Ω	Stator-rotor ratio n_{sr}	0.369

4.3.2 Stator and Rotor Current Control

Besides accelerating the damping of the stator natural flux, limiting the rotor and stator current is another major task for the DFIG systems under grid faults. A simple control strategy is proposed F.K.A. Lima et al. [46] to limit the stator and

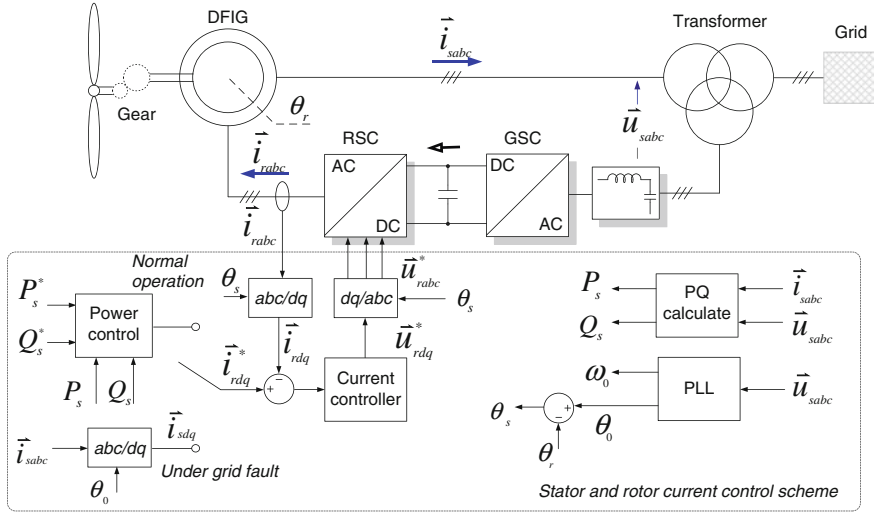


Fig. 43 Control scheme of the stator and rotor current control for a DFIG WTS

rotor currents, by applying the stator current as the rotor current reference under grid faults, which is shown in (25).

$$\bar{i}_r^* = \bar{i}_s \quad (25)$$

Therefore, the rotor current in the natural and forced machine models may be derived from (25) and (13), and expressed as (26).

$$\bar{i}_{rm} = \frac{\bar{\psi}_{sn}}{L_s + L_m} \quad \text{and} \quad \bar{i}_{rf} = \frac{\bar{\psi}_{sf}}{L_s + L_m} \quad (26)$$

If the voltage rate of the RSC is large enough to control the rotor current as expressed in (26), the rotor current during grid fault can be limited. However, since the rotor natural current here has the same direction with the stator natural flux, the damping ability on the stator natural flux may not be as good as that in demagnetizing current control. The control scheme of this control strategy is shown in Fig. 43. During the voltage dips, the rotor current reference is switched from the output of the outer power control loop to the stator current. The control structure is simple and the flux observer is not needed.

The simulation results of a 1.5 MW DFIG WTS with stator and rotor current control is shown in Fig. 44a, and also compared with the normal vector control (Fig. 44b). The rotor current is significantly reduced by the stator and rotor current control. However, the damping of the natural flux is not accelerated. The torque fluctuation is smaller than that in the demagnetizing current control, and almost the same as that in the normal vector control.

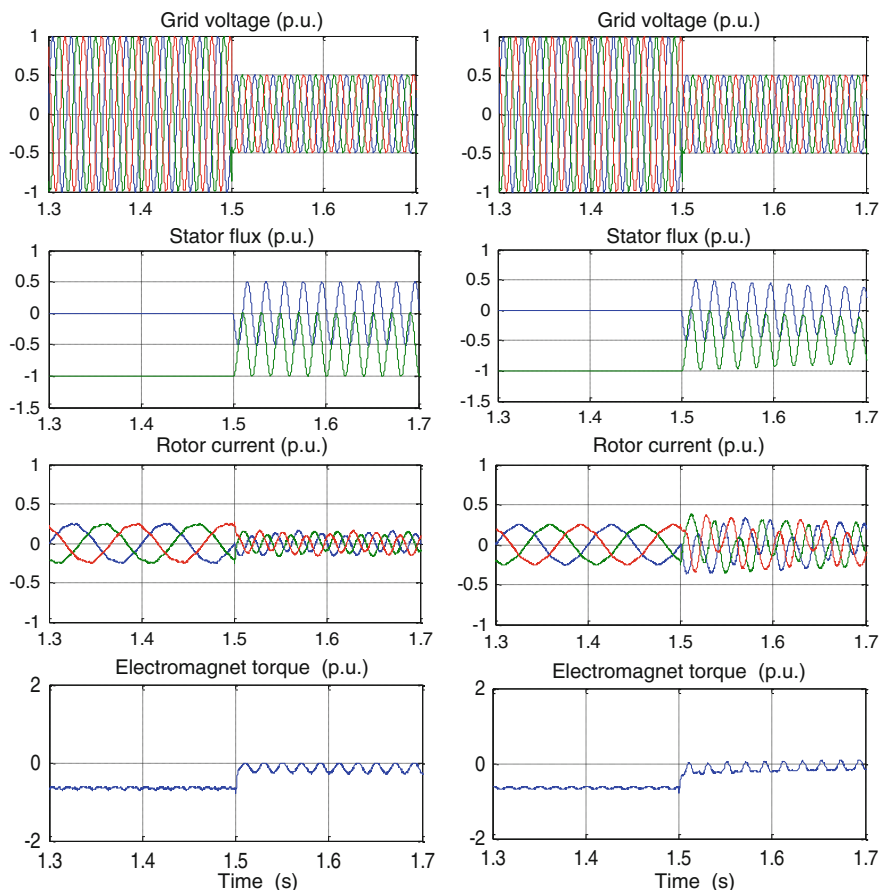


Fig. 44 Simulation results of a 1.5 MW DFIG WTS under 50 % symmetrical voltage dips: **a** with stator and rotor current control and **b** with normal vector control

4.4 Hardware Protections for the DFIG Under Grid Faults

Although it is a cost-efficient way to ride through the grid fault by applying advanced control strategies, the hardware protection is still necessary under serious voltage sags. Since the rotor EMF produced by the stator natural and negative-sequence flux may be much larger than the maximum output voltage of the RSC, the RSC may be saturated and the generator might be out of control. On the other hand, the extra power in the rotor circuit need to be dissipated as the power delivery ability of the GSC is reduced with the voltage dips. In this case, hardware solutions are necessary to protect the RSC and help the DFIG ride through grid faults.

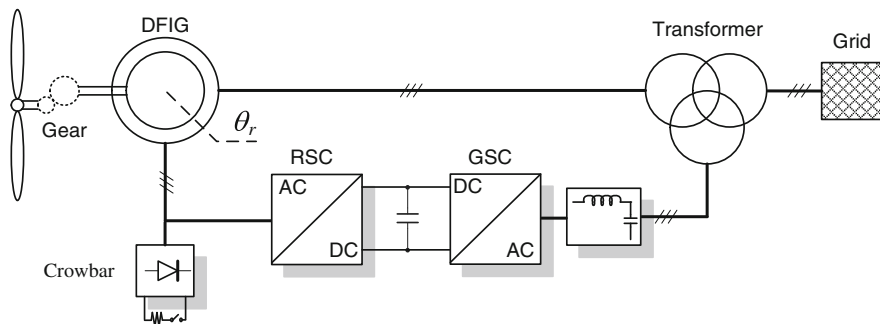


Fig. 45 A DFIG WTS with rotor side crowbar

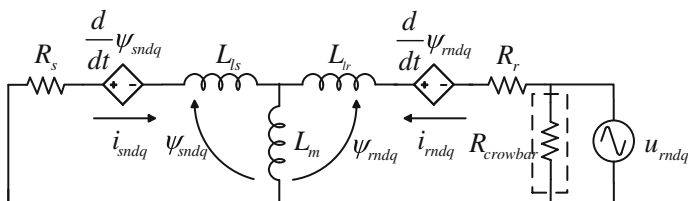


Fig. 46 Equivalent circuit of the natural machine with rotor side crowbar

4.4.1 Rotor Side Crowbar

A rotor side crowbar can short-circuit the rotor side of DFIG under grid faults with a resistance, so the rotor transient current will flow through the crowbar instead of the RSC, as shown in Fig. 45 [41]. The equivalent circuit of the natural machine in a DFIG with the rotor side crowbar is shown in Fig. 46. With the application of the rotor side crowbar, the rotor current and stator current are limited, and the damping of the stator natural flux can be accelerated.

The value of the crowbar resistance must be designed carefully to meet the FRT requirements. If the crowbar resistance is too small, the rotor and stator current will still be very large. If the crowbar resistance is too large, the voltage on the crowbar will be too high and it may give a rise to the DC-link voltage of the RSC. This may cause over-voltage on the switching devices.

Besides the additional cost, the major drawback of the crowbar is that the rotor side is short-circuited, when the crowbar is enabled. Thus, in this case, the DFIG works as a caged generator and the DFIG is out of the RSC control. Since the magnetizing current cannot be provided by the RSC, the stator will absorb reactive power from the grid, which is against the grid requirements.

To overcome these drawbacks, the rotor side crowbar can be enabled only for a short-period after the voltage dips, and then cut off from the rotor side as long as

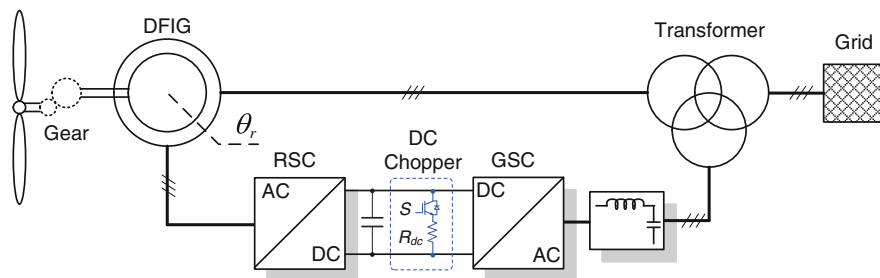


Fig. 47 A DFIG WTS with DC-chopper

the natural flux is damped. By doing so, the output voltage of RSC is large enough to control the DFIG. Advanced control schemes can be cooperated with the crowbar to shorten its operating time. However, for the asymmetrical faults, as the rotor EMF brought by the stator negative-sequence flux is so large, the crowbar has to be enabled all the time during the voltage dips.

4.4.2 DC-Chopper

In order to avoid the overvoltage on the DC-link of the RSC, a breaking chopper is usually added on the DC-link. When the DC-link voltage surpasses the limit, the DC-chopper can be connected in order to consume the energy, as it is shown in Fig. 47 [47].

If the RSC is disabled when the DC-chopper is activated at the DC-link, the DC-chopper will act as the rotor side crowbar from the rotor side point of view. The DFIG will be out of control and the stator side will absorb a large amount of reactive power from the grid. However, the DC-chopper is usually cooperated with the advanced control strategies. When the RSC is saturated and/or when the rotor EMF is too large for the RSC to handle, the DC-chopper can consume the power fed to the DC-link and thus avoid over-voltage on the DC capacitor. The safety operation is guaranteed under serious voltage dips.

The DC-chopper can also be used together with a crowbar. In this case, the rotor current can be shared between the DC-chopper and the rotor-side crowbar. The activating time of the rotor side crowbar can somehow be reduced.

4.4.3 Series Dynamic Breaking Resistor

The rotor side crowbar uses a resistor, which is parallel connected to the RSC in order to limit the rotor current. Another approach is to connect the resistor in series with the RSC in the rotor side, or with the DFIG in the stator side, or both, as it is shown in Fig. 48 [48].

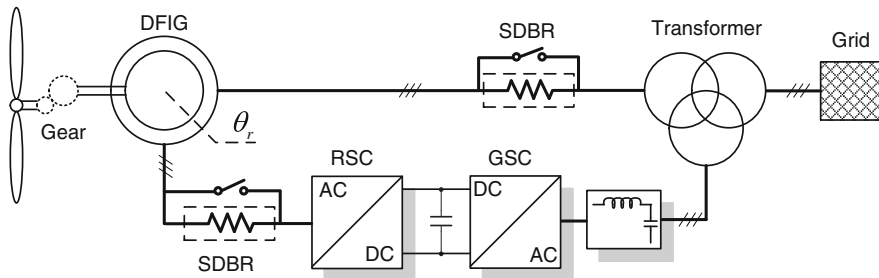


Fig. 48 A DFIG WTS with the series dynamic breaking resistor

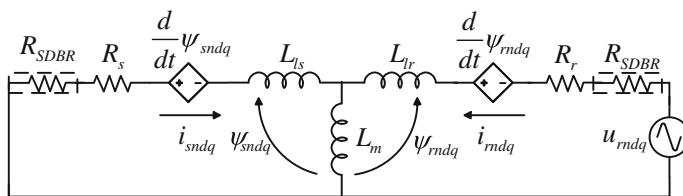


Fig. 49 Equivalent circuit of the natural machine with stator and rotor SDBR

This so-called Series Dynamic Breaking Resistor (SDBR) can limit the rotor current, and accelerate the damping of the stator natural flux at the same time. The equivalent circuit of the natural machine with stator and rotor SDBR is shown in Fig. 49. The stator and rotor resistance is increased by the SDBR, so the rotor and stator current can be significantly limited. Moreover, the voltage drop across the SDBR will reduce the output voltage demand of the RSC. Further, the increase of the stator resistance will accelerate the damping of the natural flux.

4.4.4 Dynamic Voltage Restorer and Other Wind Farm Solutions

The Dynamic Voltage Restorer (DVR) uses a converter in series connected with the stator side of the DFIG in order to compensate voltage dips, as shown in Fig. 50. In normal situation, the output voltage of the DVR is controlled to be zero. When the grid voltage drops, the DVR will generate a voltage to compensate the voltage dips, so the stator side will not “see” the voltage dips and no stator natural or negative sequence flux will be introduced [49, 50]. The DVR can also be placed between the transformer and the grid, so that the GSC will not be influenced by the voltage dip either.

Since the stator voltage of the DFIG will not decrease with the compensation of the DVR, no special control strategies are needed for the RSC. However, the major drawback of the DVR is its high cost. An additional converter is required together

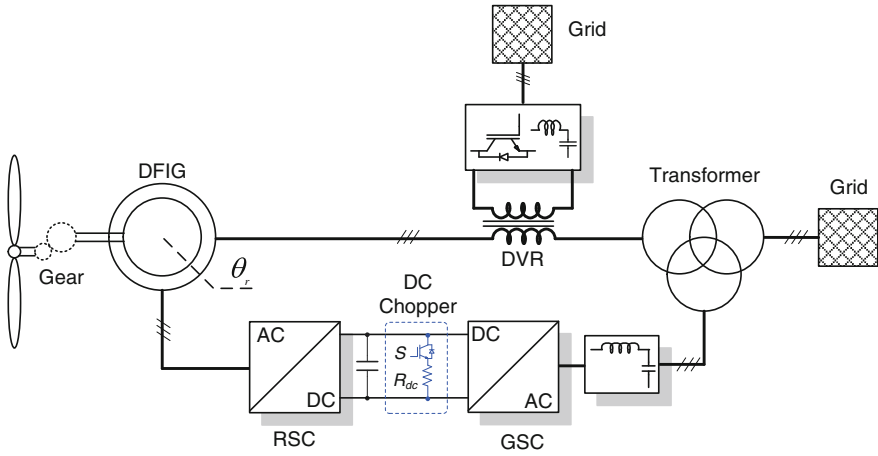


Fig. 50 A DFIG WTS with a dynamic voltage restorer

with a transformer of large power rating, which is connected to the stator side. The DVR can also be connected to the AC-bus of wind farms, known as Static Synchronous Series Compensator (SSSC). With an accurate control, all the WTSs in a wind farm will experience only a very short time of voltage dips, and the stator voltage remains in normal during the operation.

Moreover, the STATCOM has been widely used in modern wind farms, since it can provide reactive power support during the voltage dips. It can also rise the line voltage, and compensate the reactive power absorbed by the DFIG when the crowbar is activated.

5 Summary

To meet the imperative demand of a clean and reliable electricity generation, more efforts have been made on the integration of solar and wind energies. In this case, the grid stability and robustness may be violated due to the intermittency and interaction of the solar and wind renewables. Advanced and intelligent control solutions applied to the power electronics systems, discussed in this chapter, can enable the power conversion efficiently and reliably. As shown in this chapter, the power ratings range from several kilowatts to few megawatts, which covers residential PV applications and megawatts wind power plants. Related grid demands, which will be more stringent, have been presented firstly.

In respect to single-phase applications, mostly residential PV systems, advanced and intelligent control strategies have been discussed considering a wide-scale adoption of photovoltaic energy. For instance, the LVRT, which has been a basic requirement for wind turbine systems, has been investigated for

low-voltage PV systems. Three possible reactive power injection strategies can be adopted for a single-phase PV system under grid faults: (a) constant peak current control, (b) constant active current control and (c) constant average active power control strategy. In order to further increase the PV penetration level, a constant power generation control strategy has been developed in this chapter.

For commercial applications, the PV systems also include central inverters with high power ratings (e.g. tens to hundreds of kilowatts), forming three-phase systems. The control strategies for such systems are similar to those for the grid-side converter in WTs. The differences lie in the control of the rotating machines, e.g. two commonly used generators—PMSG and DFIG, and the injection of the positive- and/or negative-sequence currents under grid faults. Four major strategies are available for such systems: (a) unity power factor control, (b) positive sequence control, (c) constant active power control and (d) constant reactive power control. The implementations of such control strategies can be done in dq -, $\alpha\beta$ -, and abc -reference frames. Improvements of LVRT for DFIG based WTs by means of hardware protection solutions have also been discussed in this chapter, like using the rotor side crowbar, the DC-chopper, the SDBR and the DVR.

References

1. IEEE Std 929-2000, *IEEE Recommended practice for utility interface of photovoltaic (PV) systems*, Apr 2000, ISBN 0-7381-1934-2 SH94811
2. F. Blaabjerg, Z. Chen, S.B. Kjaer, Power electronics as efficient interface in dispersed power generation systems. *IEEE Trans. Power Electron.* **19**(5), 1184–1194 (2004)
3. F. Blaabjerg, R. Teodorescu, M. Liserre, A.V. Timbus, Overview of control and grid synchronization for distributed power generation systems. *IEEE Trans. Ind. Electron.* **53**(5), 1398–1409 (2006)
4. Y. Xue, K.C. Divya, G. Griepentrog, M. Liviu, S. Suresh, M. Manjrekar, Towards next generation photovoltaic inverters, in *Proceedings of ECCE'11*, pp. 2467–2474, 17–22 Sept 2011
5. Y. Yang, P. Enjeti, F. Blaabjerg, H. Wang, Suggested grid code modifications to ensure wide-scale adoption of photovoltaic energy in distributed power generation systems, in *Proceedings of IEEE IAS Annual Meeting*, pp. 1–8, 6–11 Oct 2013
6. Comitato Elettrotecnico Italiano, CEI 0-21: Reference technical rules for connecting users to the active and passive LV distribution companies of electricity. <http://www.ceiweb.it/>
7. E. ON GmbH, Grid Code—High and extra high voltage. <http://www.eon-netz.com/>
8. H. Kobayashi, Fault ride through requirements and measures of distributed PV systems in Japan, in *Proceedings of IEEE-PES General Meeting*, pp.1–6, 22–26 Jul 2012
9. D. Rosenwirth, K. Strubbe, Integrating variable renewables as Germany expands its grid, 2013. <http://www.renewableenergyworld.com/>
10. Technical Regulation 3.2.5, Technical regulation 3.2.5 for wind power plants with a power output greater than 11 kW, *Energinet*, 2011. <http://www.energinet.dk>
11. GB/T-19963-2011, Technical rule for connecting wind farm to power system, *The National Standard of China*, 2012. <http://www.sac.gov.cn/>
12. Transmission Code 2007, Networks and system rules of the german transmission system operators, *VDN-e.v. beim VDEW*, Aug 2007. <http://www.vdn-berlin.de>

13. Resolution P.O. 12.3, Response requirements against voltage dips in wind installations, *Red Electrical*, Mar 2006. <http://www.ree.es>
14. Requirements for offshore grid connections in the E.ON nets network, *E.ON*, 2008. <http://www.eon-netz.com>
15. S.B. Kjaer, J.K. Pedersen, F. Blaabjerg, A review of single-phase grid-connected inverters for photovoltaic modules. *IEEE Trans. Ind. Appl.* **41**(5), 1292–1306 (2005)
16. R. Teodorescu, M. Liserre, P. Rodriguez, *Grid Converters for Photovoltaic and Wind Power Systems*. (Wiley, Chichester, 2011)
17. A. Timbus, M. Liserre, R. Teodorescu, P. Rodriguez, F. Blaabjerg, Evaluation of current controller for distributed power generation systems. *IEEE Trans. Power Electron.* **24**(3), 654–664 (2009)
18. S.A. Khajehoddin, M. Karimi-Ghartemani, A. Bakhshai, P. Jain, A power control method with simple structure and fast dynamic response for single-phase grid-connected DG systems. *IEEE Trans. Power Electron.* **28**(1), 221–233 (2013)
19. S. Xu, J. Wang, J. Xu, A current decoupling parallel control strategy of single-phase inverter with voltage and current dual closed-loop feedback. *IEEE Trans. Ind. Electron.* **60**(4), 1306–1313 (2013)
20. M. Ciobotaru, R. Teodorescu, F. Blaabjerg, Control of single-stage single-phase PV inverter, in *Proceedings of EPE'05*, pp. P.1–P.10, 2005
21. Y. Yang, F. Blaabjerg, Z. Zou, Benchmarking of grid fault modes in single-phase grid-connected photovoltaic systems. *IEEE Trans. Ind. Appl.* **49**(5), 2167–2176 (2013)
22. Y. Yang, F. Blaabjerg, Low voltage ride-through capability of a single-stage single-phase photovoltaic system connected to the low-voltage grid. *Int. J. Photoenergy* **2013**, 9 (2013). Open Access. <http://dx.doi.org/10.1155/2013/257487>
23. Y. Yang, F. Blaabjerg, H. Wang, Low voltage ride-through of single-phase transformerless photovoltaic inverters. *IEEE Trans. Ind. Appl.*, May/June 2014 <http://dx.doi.org/10.1109/TIA.2013.2282966>
24. O.C. Montero-Hernandez, P.N. Enjeti, A fast detection algorithm suitable for mitigation of numerous power quality disturbances. *IEEE Trans. Ind. Appl.* **41**(6), 1684–1690 (2005)
25. Y. Yang, F. Blaabjerg, H. Wang, Constant power generation of photovoltaic systems considering the distributed grid capacity, in *Proceedings of IEEE APEC'14*, Mar 2014
26. A. Ahmed, L. Ran, S. Moon, J.-H. Park, A fast PV power tracking control algorithm with reduced power mode. *IEEE Trans. Energy Conversion.* **28**(3), 565–575 (2013)
27. H. Beltran, E. Bilbao, E. Belenguer, I. Etxeberria-Otadui, P. Rodriguez, Evaluation of storage energy requirements for constant production in PV power plants. *IEEE Trans. Ind. Electron.* **60**(3), 1225–1234 (2013)
28. C. Fitzer, M. Barnes, P. Green, Voltage sag detection technique for a dynamic voltage restorer. *IEEE Trans. Ind. Appl.* **40**(1), 203–212 (2004)
29. E. Twining, D.G. Holmes, Grid current regulation of a three-phase voltage source inverter with an *LCL* input filter. *IEEE Trans. Power Electron.* **18**(3), 888–895 (2003)
30. A.G. Yepes, F.D. Freijedo, O. Lopez, J. Doval-Gandoy, Analysis and design of resonant current controllers for voltage-source converters by means of Nyquist diagrams and sensitivity function. *IEEE Trans. Ind. Electron.* **58**(11), 5231–5250 (2011)
31. K. Ma, M. Liserre, F. Blaabjerg, Power controllability of three-phase converter with unbalanced AC source, in *Proceedings of IEEE APEC'13*, pp. 342–350, Mar 2013
32. Z. Chen, J.M. Guerrero, F. Blaabjerg, A review of the state of the art of power electronic for wind turbines. *IEEE Trans. Power Electron.* **24**(8), 1859–1875 (2009)
33. M. Liserre, R. Cardenas, M. Molinas, J. Rodriguez, Overview of multi-MW wind turbine and wind parks. *IEEE Trans. Ind. Electron.* **58**(4), 1081–1095 (2011)
34. F. Blaabjerg, M. Liserre, K. Ma, Power electronics converters for wind turbine systems. *IEEE Trans. Ind. Appl.* **48**(2), 708–719 (2012)
35. M. Chinchilla, S. Arnaltes, J.C. Burgos, Control of permanent-magnet generators applied to variable-speed wind-energy systems connected to the grid. *IEEE Trans. Energy Convers.* **21**(1), 130–135 (2006)

36. J.F. Conroy, R. Watson, Low-voltage ride-through of a full converter wind turbine with permanent magnet generator. *IET Renew. Power Gener.* **1**(3), 182–189 (2007)
37. X. Yuan, F. Wang, D. Boroyevich, Y. Li, R. Burgos, DC-link voltage control of a full power converter for wind generator operating in weak-grid systems. *IEEE Trans. Power Electron.* **24**(9), 2178–2192 (2009)
38. K.H. Kim, Y.C. Jeung, D.C. Lee, H.G. Kim, LVRT scheme of PMSG wind power system based on feedback linearization. *IEEE Trans. Power Electron.* **27**(5), 2376–2384 (2012)
39. R. Pena, J.C. Clare, G.M. Asher, Doubly fed induction generator using back-to-back PWM converters and its application to variable speed wind-energy generation. *Proc. Inst. Elect. Eng.—Elect. Power Appl.* **143**(3), 231–241 (1996)
40. G. Abad, J. Lopez, M.A. Rodriguez, L. Marroyo, G. Iwanski, *Doubly Fed Induction Machine, Modeling and Control for Wind Energy Generation*, (Wiley, Hoboken, 2011)
41. J. Morren, S.W.H. De Haan, Ride through of wind turbines with doubly-fed induction generator during a voltage dip. *IEEE Trans. Energy Convers.* **20**(2), 435–441 (2005)
42. J. Lopez, E. Gubia, P. Sanchis, X. Roboam, L. Marroyo, Wind turbines based on doubly fed induction generator under asymmetrical voltage dips. *IEEE Trans. Energy Convers.* **23**(1), 321–330 (2008)
43. J. Lopez, P. Sanchis, X. Roboam, L. Marroyo, Dynamic behavior of the doubly fed induction generator during three-phase voltage dips. *IEEE Trans. Energy Convers.* **22**(3), 709–718 (2007)
44. D. Xiang, L. Ran, P.J. Tavner, S. Yang, Control of a doubly-fed induction generator in a wind turbine during grid fault ride-through. *IEEE Trans. Energy Convers.* **21**(3), 652–662 (2006)
45. S. Hu, X. Lin, Y. Kong, X. Zhou, An improved low-voltage ride-through control strategy of doubly fed induction generator during grid faults. *IEEE Trans. Power Electron.* **26**(12), 3653–3665 (2011)
46. F.K.A. Lima, A. Luna, P. Rodriguez, E.H. Watanabe, F. Blaabjerg, Rotor voltage dynamics in the doubly fed induction generator during grid faults. *IEEE Trans. Power Electron.* **25**(1), 118–130 (2010)
47. I. Erlich, J. Kretschmann, J. Fortmann, S.M. Engelhardt, H. Wrede, Modeling of wind turbines based on doubly-fed induction generators for power system stability studies. *IEEE Trans. Power System* **22**(3), 909–919 (2007)
48. M. Rahimi, M. Parniani, Coordinate control approaches for low-voltage ride-through enhancement in wind turbines with doubly fed induction generators. *IEEE Trans. Energy Convers.* **25**(3), 873–883 (2010)
49. O. Abdel-Baqi, A.R. Nasiri, A dynamic LVRT solution for doubly fed induction generators. *IEEE Trans. Power Electron.* **25**(1), 193–196 (2010)
50. S. Zhou, J. Liu, L. Zhou, Y. Zhu, X. Yang, Sag detection algorithm for dynamic voltage restorer used in wind farms under unbalanced and distorted grid voltage conditions, in *Proceedings of ECCE Asia*, pp. 601–606, 3–6 June 2013

Advanced and Intelligent Control in Power Electronics
and Drives

Orłowska-Kowalska, T.; Blaabjerg, F.; Rodríguez, J. (Eds.)

2014, XX, 410 p. 284 illus., 161 illus. in color.,

Hardcover

ISBN: 978-3-319-03400-3